Switching from Autopilot to the driver
A transient performance analysis

Ramanathan Venkita, Seshan

Award date:
2018

Switching from Autopilot to the driver : A transient performance analysis

Seshan Ramanathan Venkita

DC2018.073

ID : 1033486
Program : Automotive Technology, M.Sc

Supervisors,
TU/e : Prof. Dr. H. (Henk) Nijmeijer
TNO : ir. D.M.C. (Dehlia) Willemsen, Dr. M. (Mohsen) Alirezaei

Technische Universiteit Eindhoven University of Technology
Dynamics and Control (D&C)
Department of Mechanical Engineering

TNO innovation for life
Department of Integrated Vehicle Safety (IVS)
Traffic and Transport Unit

Version : Final

August 5, 2018, Eindhoven

Technische Universiteit
Eindhoven
University of Technology

Declaration concerning the TU/e Code of Scientific Conduct for the Master's thesis

I have read the TU/e Code of Scientific Conduct[i].

I hereby declare that my Master's thesis has been carried out in accordance with the rules of the TU/e Code of Scientific Conduct

Date

5/8/2018

Name

SESHAN RAMANATHAN VENKITA

ID-number

1033486

Signature

Seshan

Submit the signed declaration to the student administration of your department.

[i] See: http://www.tue.nl/en/university/about-the-university/integrity/scientific-integrity/
The Netherlands Code of Conduct for Academic Practice of the VSNU can be found here also.
More information about scientific integrity is published on the websites of TU/e and VSNU

CONTENTS

LIST OF FIGURES

LIST OF TABLES

Switching from Autopilot to the driver : A transient performance analysis

***Abstract*—One of the main safety concerns associated with semi-autonomous vehicles is the sharing of control between a human driver and an autonomous driving system. Even with an attentive driver, such switches in control may pose a threat to the safety of the driver and the surrounding vehicles. The aim of this study is to develop an indicator that can measure the level of safety during a driver take-over, using knowledge about the system known *a priori*. A model based approach is used to analyze the system with special focus on the lateral dynamics of the vehicle. The driver and the vehicle are modeled as linear systems and a path tracking controller is used to serve as an autonomous system. With this structure, shared control is studied as a switched system, in which the vehicle's lateral control switches between the driver and the autonomous system. A bound on the transient dynamics that arise due to a switch is derived, using the induced $\mathcal{L}_\infty$ norms. This bound is then used to formulate an indicator that checks if the states/outputs of interest lie within their acceptable limits. A comparison with simulation results has shown that the indicator successfully captures the effect of different system parameters on take-over safety, although in a slightly conservative manner. This indicator can be further developed as a tool to be used in the design and evaluation of shared/multi-modal control systems in future vehicles.**

I. Introduction

Autonomous driving technology has the potential to become a game changer in the mobility industry of the 21st century [3]. People's perception of driving and transportation as a whole stand the chance of being transformed, given the far reaching opportunities for innovation that these systems have opened up. As of today, automotive manufacturers and suppliers have developed systems that are capable of achieving varying levels of driving autonomy, most of which fall under the SAE levels 2 and 3 of automation [4], while some level 4 systems are also being experimented by ride hailing companies. Overall, there are two schools of thought within the industry, one that believes that semi-autonomous driving technology is crucial towards building people's trust in autonomous systems, while the other advocates for a direct shift to fully autonomous systems. It is, however, expected that semi-autonomous systems will have their place on the road until technology, infrastructure and regulation have matured enough to give way to fully autonomous systems [4].

The main challenge associated with the development of semi-autonomous systems is the sharing of control between the driver and the autonomous system. When the autonomous system reaches its boundaries it has to alert the driver and hand over control safely [5], while the driver can also manually take or give control to the system. The driver's actions following a transfer of control is the major threat to safety, which has been proven by a number of studies in literature [5]–[8]. In [7] the driver's behaviour during a transfer of control is studied by observing his or her reaction time to a 'take-over' request from the vehicle. The results show that, when the time given to resume control is reduced, decision making and reactions are faster but are generally worse in quality. A similar study [8] measured the frequency content of the steering angle and the lateral position of the vehicle after a transfer of control, which has shown that it takes around 35 - 40 seconds for the driver to stabilize the lateral control of the vehicle after resuming control. These studies help in understanding certain aspects of the driver's reactions from a human-factors perspective, but do not provide a systematic approach to study such scenarios. This research tries to bridge this gap by proposing a model based method that can be used to assess the safety of a transition of control.

A classification of the different types of transitions of control, as presented in Fig. 1, helps in developing a better understanding of the problem at hand.

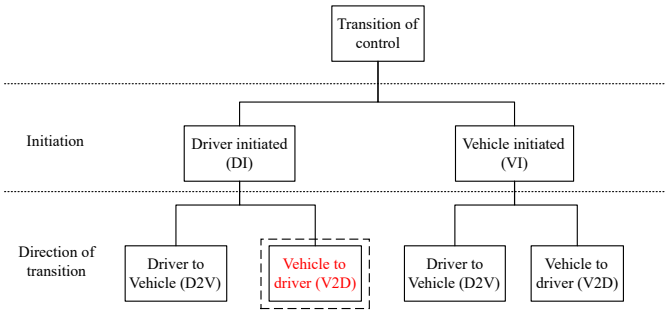

Fig. 1. Classification of the different types of transitions, the dotted box highlights the focus of this research

The classification is done in two levels, based on the initiation and the direction of transition, as shown in Fig. 1. Based on initiation, the transition can be classified as 'Driver Initiated (DI)' or 'Vehicle Initiated (VI)' transitions and the direction of transition can be either from the driver to the vehicle (D2V) or from the vehicle to the driver (V2D).

This results in four classes of transitions, DI-D2V, DI-V2D, VI-V2D and VI-D2V transitions. Among these, the VI-V2D transitions have a higher potential for danger, compared to the other types of transitions. This is because in VI-V2D transitions, the driver is likely to have a much lower level of situational awareness when the transition is initiated. This is attributed to the low workload during the autonomous driving mode, in which, not much information

related to the driving task has to be processed by the driver. This diminished situational awareness will not be immediately restored on switching to manual driving, posing a greater threat to a safe transition [6].

However, in a DI type of transition, factors such as the driver's response to a take-over request from the vehicle and bringing him/her back to the driving loop, have a lower influence making the problem easier to analyze using mathematical models. Hence, this research tries to take a first step towards addressing the safety concerns during a transition of control by focusing on the DI-V2D type transitions, also termed in this report as a 'take-over'.

A. Methodology and assumptions

A take-over is studied in this research with special attention to the lateral dynamics of the vehicle, assuming that the driver takes over control of the vehicle only through the steering wheel. A model based approach is followed, with the driver and the vehicle modeled as linear systems. A path tracking controller is used to emulate an autonomous driving system and shared control is studied as a switched system, in which the vehicle's lateral control switches between the driver and the autonomous system. The longitudinal speed of the vehicle is taken as a constant, as it is assumed to be controlled by a cruise control system with a bandwidth much lower than than that of the lateral controller.

It is also assumed that after a switch from the autonomous system to the driver the system stays in the manual mode for a sufficiently long period of time. This assumption is made because it is of interest in this research to focus on the transient dynamics that are present for a finite time interval following a switch.

Having narrowed down the focus area of this research, the next part of this section highlights the objectives of the work.

B. Research objectives and supporting literature

The objective of this research is to develop a 'switching performance indicator' that can be used to evaluate the safety of a switch from the autonomous system to the driver. It is required that this indicator quantifies the safety critical aspects of the transient dynamics that arise due to a switch. These safety critical aspects can be the amplitude, frequency content or settling time of the signal (state/output of the system) being studied. As a first step in this direction, this research focuses on deriving a performance indicator that can provide a bound on the amplitude of the transient dynamics, using knowledge about the system known a priori.

Some studies in literature have developed tools that could help in achieving the objective of this research. In [9] an $\mathcal{L}_p$ string stability condition is proposed for cascaded systems using its input-output properties. The $\mathcal{L}_2$ and $\mathcal{L}_\infty$ induced gains are used to arrive at corresponding string stability conditions. An analogy can be drawn here, between notions of string stability and that of a switching performance indicator, as both are measures of system performance, applicable in a finite time domain. These induced gains could be used in the context of switched systems to derive bounds on the states/outputs based on the system dynamics, as it will be discussed in the subsequent sections.

A Linear Matrix Inequality (LMI) based approach to determine a bound on the overshoot for the step responses of linear systems is discussed in [10]. Since a step input can be considered as a worst case input for the application at hand, a bound on the overshoot would also give a bound on the transients for any general input (provided the step input is scaled proportional to the amplitude of the actual input). However, since the LMIs are derived from Lyapunov conditions, it can be expected that these bounds would be quite conservative.

It is to be noted here that, notions of stability of the switched system are not investigated in this research, as it is assumed that the system stays in the manual mode for a sufficiently long duration after a switch. This assumption puts the system into a class of 'slow-switched' systems, for which stability can be guaranteed by defining constraints on the switching signal, provided the individual subsystems are stable. A lower bound on the average dwell time between consecutive switches is proposed in [11], which guarantees stability for such systems. A specific application of this result to prove the stability of switches between the manual and automated driving is also presented in [12].

The next section discusses the overall structure of the system and the models used for each of the system components. Section III presents an analysis on the transient dynamics and the different methods to define a bound on it. In Section IV, a comparison is done between simulation results and the obtained performance indicators. Finally, conclusions and recommendations to improve on the results are discussed in Section V.

II. Modeling a take-over

A. Structure of the switched system

As discussed in the previous section, shared control between the driver and the autonomous system can be modelled as a switched system, which is depicted in the block diagram shown in Fig. 2. It can be seen that the vehicle is controlled either by the driver or the path tracking controller and a transfer of control between the two can be seen as a switch between the two control modes. In the autonomous mode, the path tracking controller computes the set point steering angle (δ_{set}) which is realised by a steering actuator. In the manual mode, the driver's perception and mental computation of the desired steering input (δ_{des}) can be seen as a controller, while the actuation is carried out by the human neuromuscular system, which is represented by the block 'Driver dynamics' in Fig. 2. The models for each

of these components are discussed in the subsequent parts of this section.

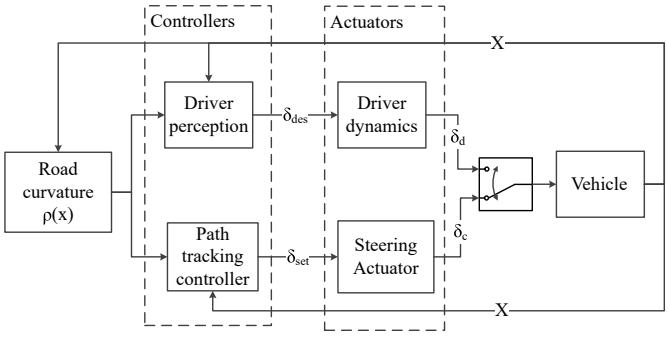

Fig. 2. Block diagram - overall system

B. Vehicle model

The lateral dynamics of the vehicle is modelled using a single track vehicle model [13], shown in Fig. 3.

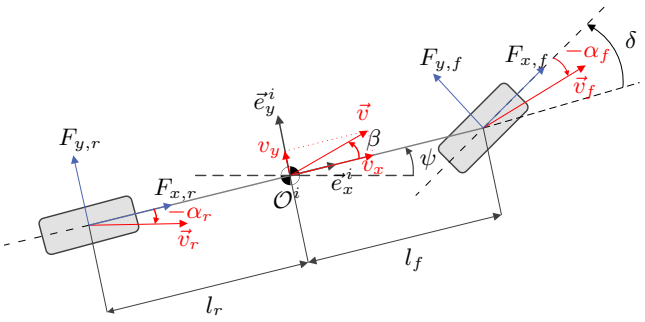

Fig. 3. Single track vehicle model

The notations used in the Fig. 3 along with the vehicle parameters that will be used in this section are listed in Table I.

The lateral tyre forces ($F_{y,f}$ and $F_{y,r}$) are assumed to be in their linear region, meaning that they are linearly dependent on the corresponding tyre slip angles (α_f and α_r), given by

$$\begin{aligned} F_{y,f} &= -C_f \alpha_f \\ F_{y,r} &= -C_r \alpha_r \end{aligned} \tag{1}$$

This assumption is true for 'small' slip angles that correspond to lateral accelerations typically less than $\approx 4m/s^2$ [13]. From Fig. 3, the slip angles can be expressed as :

$$\begin{aligned} \alpha_f &= \left(\frac{v_y + l_f \omega_z}{v_x} \right) - \delta \\ \alpha_r &= \left(\frac{v_y - l_r \omega_z}{v_x} \right) \end{aligned} \tag{2}$$

where, the yaw rate $\omega_z := \dot{\psi}$. The equations of motion for the lateral and yaw motion of the single track model are given by :

$$l_f F_{y,f} - l_r F_{y,r} = I_{zz} \dot{\omega_z} \tag{3}$$

$$m(\dot{v_y} + v_x \omega_z) = F_{y,f} + F_{y,r} \tag{4}$$

Note that the steering angle δ is assumed to be small while deriving (3) and (4). The equations of motion for the longitudinal direction is not considered because the longitudinal velocity is assumed to be a constant as discussed in Section I-A.

Substituting (1) and (2) in the equations of motion (3), (4) and by collecting the coefficients of v_y, ω_z and δ,

$$\begin{aligned} \dot{v_y} &= -\frac{C_f + C_r}{m v_x} v_y - \left(\frac{l_f C_f - l_r C_r}{m v_x} + v_x \right) \omega_z + \frac{C_f}{m} \delta \\ \dot{\omega_z} &= -\frac{l_f C_f - l_r C_r}{I_{zz} v_x} v_y - \frac{l_f^2 C_f + l_r^2 C_r}{I_{zz} v_x} \omega_z + \frac{l_f C_f}{I_{zz}} \delta \end{aligned} \tag{5}$$

TABLE I
VEHICLE PARAMETERS AND VARIABLES (TOYOTA PRIUS TEST PLATFORM AT TNO [2])

Variable	Description	
v_y	Lateral velocity [m/s]	
ω_z	Yaw velocity [rad/s]	
ψ	Heading angle [rad]	
v_x	Vehicle forward velocity [m/s]	
δ	Steering angle [rad]	
$F_{x,f}, F_{x,r}$	Front and rear longitudinal tyre forces[N]	
$F_{y,f}, F_{y,r}$	Front and rear lateral tyre forces[N]	
β	Body slip angle [rad]	
$\vec{v}_f, \vec{v}_r$	Front and rear wheel center velocity vectors	
$\vec{v}$	Velocity vector of the center of mass	
$\mathcal{O}^i$	Center of mass of the vehicle	
$\underline{\vec{e}}^i = [\vec{e}_x^i, \vec{e}_y^i]^T$	Vehicle fixed reference frame at $\mathcal{O}^i$	
α_f, α_r	Wheel slip angles [rad]	
Parameter	**Description**	**Value**
C_f	Front axle cornering stiffness[Nm/rad]	9.84×10^4
C_r	Rear axle cornering stiffness[Nm/rad]	1.98×10^5
l_f	Position of CG from front axle [m]	1.11
l_r	Position of CG from rear axle [m]	1.59
I_{zz}	Moment of inertia about the Z-axis [Kgm^2]	2865.6
m	Mass of the vehicle [Kg]	1625

This vehicle model is intended to be used for the purpose of path tracking, which necessitates the definition of the path tracking errors that are depicted in Fig. 4. The curve $\mathcal{C}$ in Fig. 4 represents a reference path, with $\mathcal{O}^s$ being the point on the curve along the $\vec{e}_y^i$ direction. The set of vectors $\underline{\vec{e}}^s = [\vec{e}_x^s \quad \vec{e}_y^s]^T$ represents a reference frame centered at $\mathcal{O}^s$ with $\vec{e}_x^s$ tangent to the curve at $\mathcal{O}^s$. Furthermore, $\underline{\vec{e}}^g = [\vec{e}_x^g \quad \vec{e}_y^g]^T$ is a ground fixed reference frame centered at a stationary point $\mathcal{O}^g$.

With this setting, two types of tracking errors are defined [14] :

- Angular error (ψ_e) : Difference between the vehicle's heading angle (ψ) and θ_s, where θ_s is the orientation of $\vec{e}_x^s$ with respect to $\vec{e}_x^g$, i.e. $\psi_e = \theta_s - \psi$.
- Distance error (y_e) : The distance of the point $\mathcal{O}^s$ from the center of mass of the vehicle along the $\vec{e}_y^i$ direction. i.e. $y_e = \|\vec{r}_{\mathcal{O}^s/\mathcal{O}^i}\|$.

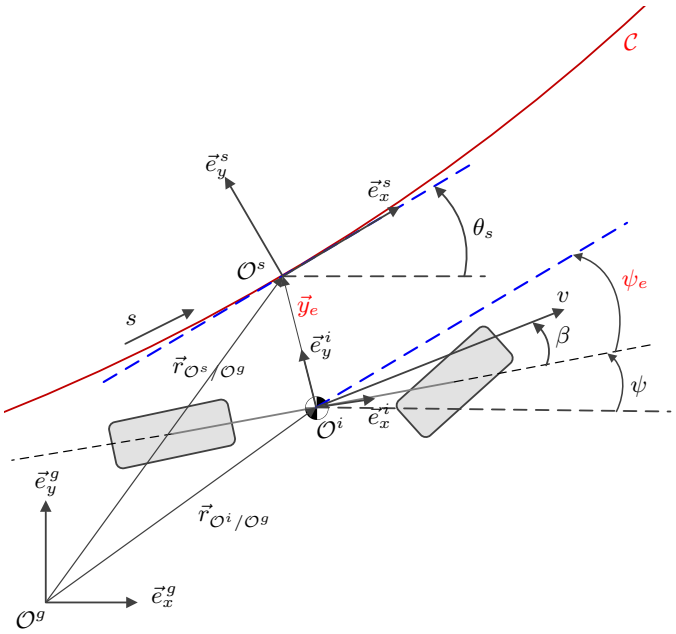

Fig. 4. Geometric representation of the tracking errors $\vec{y}_e$ and ψ_e

The center of mass of the vehicle is taken as the reference for defining these errors because it is the point of interest that has to follow the reference path.

The dynamics of the angular error can be derived by differentiating the angular error,

$$\dot{\psi}_e = \dot{\theta}_s - \omega_z \tag{6}$$

where, $\dot{\theta}_s$ can be approximated using the curvature (ρ) of the reference path,

$$\rho := \frac{\partial \theta_s}{\partial s} = \frac{\partial \theta_s}{\partial t} \Big/ \frac{\partial s}{\partial t} \approx \frac{\dot{\theta}_s}{v_x} \tag{7}$$

where s is the distance traveled along the curve $\mathcal{C}$ and for small values of ψ_e, $\partial s/\partial t$ is approximated as the forward velocity v_x. The angular error dynamics in (6) can be written using (7) as :

$$\dot{\psi}_e \approx v_x \rho - \omega_z \tag{8}$$

The dynamics of the distance error (y_e) can be derived using vector summation from Fig. 4, given by :

$$\dot{\vec{r}}_{\mathcal{O}^s/\mathcal{O}^g} = \dot{\vec{r}}_{\mathcal{O}^i/\mathcal{O}^g} + \dot{\vec{r}}_{\mathcal{O}^s/\mathcal{O}^i} \tag{9}$$

According to the single track vehicle model in Fig. 3,

$$\dot{\vec{r}}_{\mathcal{O}^i/\mathcal{O}^g} = \begin{bmatrix} v_x & v_y \end{bmatrix} \underline{\vec{e}}^i, \quad \underline{\vec{e}}^i = \begin{bmatrix} \vec{e}^i_x & \vec{e}^i_y \end{bmatrix}^T \tag{10}$$

As $\vec{r}_{\mathcal{O}^s/\mathcal{O}^i} = y_e \vec{e}^i_y$,

$$\begin{aligned} \dot{\vec{r}}_{\mathcal{O}^s/\mathcal{O}^i} &= y_e \dot{\vec{e}}^i_y + \dot{y}_e \vec{e}^i_y \\ &= -y_e \omega_z \vec{e}^i_x + \dot{y}_e \vec{e}^i_y \end{aligned} \tag{11}$$

using $\dot{\underline{\vec{e}}}^i = \begin{bmatrix} 0 & \omega_z \\ -\omega_z & 0 \end{bmatrix} \underline{\vec{e}}^i$.

Substituting (10) and (11) in (9),

$$\dot{\vec{r}}_{\mathcal{O}^s/\mathcal{O}^g} = \begin{bmatrix} v_x - y_e \omega_z & v_y + \dot{y}_e \end{bmatrix} \underline{\vec{e}}^i \tag{12}$$

By definition $\mathcal{O}^s$ moves in the direction of $\vec{e}^s_x$, such that,

$$\begin{aligned} \dot{\vec{r}}_{\mathcal{O}^s/\mathcal{O}^g} &= \begin{bmatrix} \dot{s} & 0 \end{bmatrix} \underline{\vec{e}}^s \\ &= \begin{bmatrix} \dot{s} & 0 \end{bmatrix} R^T(\psi_e) \underline{\vec{e}}^i \\ &= \begin{bmatrix} \dot{s}\cos\psi_e & \dot{s}\sin\psi_e \end{bmatrix} \underline{\vec{e}}^i \end{aligned} \tag{13}$$

where $R(\psi_e) = \begin{bmatrix} \cos\psi_e & -\sin\psi_e \\ \sin\psi_e & \cos\psi_e \end{bmatrix}$, is the direction cosine matrix such that $\underline{\vec{e}}^i = R(\psi_e)\underline{\vec{e}}^s$.

Equating (12) and (13) element wise and eliminating $\dot{s}$ gives,

$$\dot{y}_e = -v_y + (v_x - y_e \omega_z) \tan\psi_e \tag{14}$$

for small values of ψ_e, $\tan\psi_e \approx \psi_e$ and for highway driving $v_x \gg y_e\omega_z$ resulting in,

$$\dot{y}_e \approx -v_y + v_x \psi_e \tag{15}$$

The error dynamics given by (8) and (15) along with the vehicle dynamics (5) can be together written in the state space form,

$$\begin{aligned} \dot{X} &= AX + B_1\delta + B_2\rho \\ X = \begin{bmatrix} v_y \\ \omega_z \\ y_e \\ \psi_e \end{bmatrix} \; A &= \begin{bmatrix} -\frac{C_f+C_r}{mv_x} & -\frac{l_fC_f - l_rC_r}{mv_x} - v_x & 0 & 0 \\ -\frac{l_fC_f - l_rC_r}{I_{zz}v_x} & -\frac{l_f^2C_f + l_r^2C_r}{I_{zz}v_x} & 0 & 0 \\ -1 & 0 & 0 & v_x \\ 0 & -1 & 0 & 0 \end{bmatrix}, \\ B_1 = \begin{bmatrix} \frac{C_f}{m} \\ \\ \frac{l_fC_f}{I_{zz}} \\ \\ 0 \\ 0 \end{bmatrix}, B_2 &= \begin{bmatrix} 0 \\ 0 \\ 0 \\ v_x \end{bmatrix} \end{aligned} \tag{16}$$

C. Driver model

The human driver is modelled using two components the 'Driver perception' and the 'Driver dynamics' as seen in Fig. 2. The driver perception is modelled as a feedback controller, using cognitive models of the driver from literature. These models mimic human cognitive functions that are active during driving. Several models are proposed in literature which are summarized in [15]. The 'Pursuit-Compensatory' driver model proposed in [1] is found to be most suitable for manoeuvres that are involved in highway driving because it computes the driver's desired steering angle as a the sum of a state feedback term that compensates for tracking errors and a feedforward term that aids in path following, as shown below :

$$\begin{aligned} \delta_{des} &= k_e(y_e + l_a\psi_e) + k_r\rho \\ &= K_dCX + k_r\rho \\ where, K_d = \begin{bmatrix} k_e & k_el_a \end{bmatrix}, \quad C &= \begin{bmatrix} 0 & 0 & 1 & 0 \\ 0 & 0 & 0 & 1 \end{bmatrix} \end{aligned} \tag{17}$$

here, l_a is the look ahead distance of the driver and gains k_e and k_r weigh the feedback and feedforward components respectively. Details regarding choosing values for these gains are discussed in Appendix A. This model has also been experimentally validated in [1]. Furthermore, a discussion on different control topologies for modelling human driving behaviour is also presented in Appendix A.

Once the desired steering angle is known, the physical actuation by the driver (represented by the block 'Driver dynamics' in Fig. 2) can be modelled using 'human operator models' from literature [16]. These models replicate the driver's physical response to a cognitive reference input. The 'Quasi-linear model' developed in [17], models the human operator by means of a second-order transfer function from the desired steering angle (δ_{des}) to the actual steering angle achieved by the driver (δ_d) as given below :

$$H(s) = \frac{\delta_d(s)}{\delta_{des}(s)} = \frac{k(T_L s + 1)}{(T_I s + 1)(T_N s + 1)} e^{-\tau_d s} \tag{18}$$

where, differences in the task environment and in operator properties are described by means of five independent parameters - k, T_L, T_I, T_N and τ_d. τ_d is the reaction time of the driver in response to a change in the reference path. It can be considered as the time needed to perceive and process the control input necessary. T_N is the time constant of the neuromuscular dynamics, which is the time required for the muscles in the drivers arms to receive and execute the actions from the central nervous system. T_L and T_I are time constants of the lead lag filter which depend on how well the driver is accustomed to the vehicle or knows a certain route. k is the driver gain which could be influenced by numerous factors like the driver's driving style, urgency, level of attention etc. Further details on choosing values for these parameters is discussed in Appendix A. This model is chosen because it provides the flexibility of modifying different properties of the driver, whilst fitting well in the linear control framework chosen for this study. The 'Quasi-Linear model' is also widely accepted in literature and is used by a number of studies to model human driving behaviour in different driving conditions [18].

A second order Padé approximation is used in the place of the exact time delay in (18) because it was found that the frequency responses of the transfer function in (18) and its second order Padé approximation are almost identical upto a frequency of $20Hz$, with their magnitude differing by a maximum of $10^{-5}dB$ and phase by 1° (for τ_d = $0.1sec$). Since (18) is to be used in this research only at low frequencies ($< 1Hz$), this approximation is valid and simplifies the analysis by eliminating the exponential term.

This results in a fourth order transfer function for the operator model (18), which can be written in the state space form as shown below :

$$\begin{aligned} \dot{\Delta}_d &= A_d \Delta_d + B_d \delta_{des} \\ \delta_d &= C_d \Delta_d \end{aligned} \tag{19}$$

where $\Delta_d = [\delta_{d_1} \delta_{d_2} \delta_{d_3} \delta_{d_4}]^T$ is a set of dummy variables for the minimal state space realization of (18), while A_d, B_d and C_d are the corresponding state space matrices. This results in the following closed loop dynamics for the driver-vehicle system, obtained by combining (16), (17) and (19) :

$$\begin{aligned} \dot{X}_d &= A_{dc} X_d + B_{dc} \rho \\ where,\ X_d &= \begin{bmatrix} X \\ \Delta_d \end{bmatrix}, A_{dc} = \begin{bmatrix} A & B_1 C_d \\ B_d K_d C & A_d \end{bmatrix}, \\ B_{dc} &= \begin{bmatrix} B_2 \\ B_d k_r \end{bmatrix} \end{aligned} \tag{20}$$

The next part of this section briefly discusses the path tracking controller used in this study as an autonomous system.

D. Path tracking controller

A path tracking controller with independent longitudinal and lateral control which is developed in [14], is used in this study. The longitudinal speed is assumed to be controlled by a cruise control or an equivalent system and the forward speed is assumed to be constant for the time horizon under consideration.

The steering control input to the vehicle involves a feedback (δ_{fb}) and a feedforward term (δ_{ff}). The feedforward component (δ_{ff}) is derived from the steady state solution of the single track vehicle model (5) by substituting $\omega_z = v_x/R$, which is approximately the steady state yaw rate of a vehicle driven along a path of constant radius R ($= \rho^{-1}$) at a constant forward speed v_x. This results in an expression for the steady state steering angle, used here as the feedforward component (δ_{ff}),

$$\delta_{ff} = (l + K_\delta u^2)\rho =: k_{ff}\rho \tag{21}$$

here, $l = l_f + l_r$ and the understeer coefficient K_δ in (21) is given by,

$$K_\delta = \frac{m}{l}\left(\frac{l_r}{C_f} - \frac{l_f}{C_r}\right)$$

The feedback component (δ_{fb}) is defined as a function of the tracking errors y_e and ψ_e, given by

$$\delta_{fb} = k_1 y_e + k_2 \psi_e = K_c C X \tag{22}$$

where, $K_c = \begin{bmatrix} k_1 & k_2 \end{bmatrix}$ is the feedback gain matrix. More details regarding the choice of the gains k_1 and k_2 is given in Appendix C.

Combining (22) and (21) the steering control input can be written as

$$\delta_{set} = K_c C X + k_{ff}\rho \tag{23}$$

The steering control input derived in (23) is realized through a steering actuator, which is modelled as a second

order transfer function from the set point (δ_{set}) steering angle (23) to the realized steering angle (δ_c), as given below :

$$H_a(s) = \frac{\delta_c(s)}{\delta_{set}(s)} = \frac{1}{\frac{s^2}{\omega_0^2} + \frac{2\beta_{str}}{\omega_0}s + 1} e^{-\tau_{str}s} \tag{24}$$

where, ω_0 and β_{str} are the natural frequency and the damping constant respectively and τ_{str} is the delay in the actuator. This dynamics correspond to the steering actuator system used in the Toyota Prius test platform at TNO [2].

Similar to the human operator model in (18), a second order Padé approximation is used for the delay in (24) and was found to be accurate up to $\approx 25Hz$ with maximum deviations similar to those discussed in the previous section for the human operator model. This results in a fourth order transfer function for the actuator dynamics, which can be written in the state space form as shown below :

$$\begin{aligned} \dot{\Delta_c} &= A_c\Delta_c + B_c\delta_{set} \\ \delta_c &= C_c\Delta_c \end{aligned} \tag{25}$$

where $\Delta_c = [\delta_{c_1}\delta_{c_2}\delta_{c_3}\delta_{c_4}]^T$ is a set of dummy variables for the minimal state space realization of (24), while A_c, B_c and C_c are the corresponding state space matrices. This results in the following closed loop dynamics for the controller-vehicle system, obtained by combining (5), (23) and (25) :

$$\begin{aligned} \dot{X_c} &= A_{cc}X_c + B_{cc}\rho \\ where,\ X_c = \begin{bmatrix} X \\ \Delta_c \end{bmatrix}, A_{cc} &= \begin{bmatrix} A & B_1C_c \\ B_cK_cC & A_c \end{bmatrix}, \\ B_{cc} &= \begin{bmatrix} B_2 \\ B_ck_{ff} \end{bmatrix} \end{aligned} \tag{26}$$

With the closed loop dynamics for both control modes obtained in (20) and (26), the next part of this section discusses how a switch is made between the two systems and some simulation results are presented to visualize the transient dynamics due to the switch.

E. Switching between the two modes

As discussed in Section I, a take-over is a switch from the controller-vehicle system (26) to the driver-vehicle system (20). The time instant of switch (τ_{to}) is an exogenous variable, as the switch is initiated by the driver out of his/her free will.

It is to be noted here that the states vectors X_c and X_d are not the same and for a switch from system (26) to (20), it is necessary to derive the initial conditions for system (20) from the state vector X_c at the time of switching (τ_{to}). It can be seen from (20) and (26) that the first set of states (X) are identical while the second set corresponding to the actuation dynamics (Δ_d and Δ_c) are different. The initial conditions for these states can be derived by imposing the conditions for continuity on the steering input and it's derivatives, at the instant of switching, as shown in the equations below :

$$\begin{aligned} \delta_c(\tau_{to}) &= \delta_d(\tau_{to}) \\ \dot{\delta_c}(\tau_{to}) &= \dot{\delta_d}(\tau_{to}) \\ \ddot{\delta_c}(\tau_{to}) &= \ddot{\delta_d}(\tau_{to}) \\ \dddot{\delta_c}(\tau_{to}) &= \dddot{\delta_d}(\tau_{to}) \end{aligned} \tag{27}$$

Continuity up to the third derivative of the steering angle is imposed in (27), since the the vectors Δ_d and Δ_c are four dimensional.

From (19) we know,

$$\delta_d = C_d\Delta_d = [0, 0, 0, 0, C_d]X_d =: C_{\Delta_d}X_d \tag{28}$$

similarly, from (25) we know

$$\delta_c = C_c\Delta_c = [0, 0, 0, 0, C_c]X_c =: C_{\Delta_c}X_c \tag{29}$$

Taking derivatives of (28) and (29) and substituting them in (27) we obtain an expression for the initial conditions of the driver-vehicle system (20) as :

$$X_d(\tau_{to}) = E^{-1}(FX_c(\tau_{to}) + GP(\tau_{to})) \tag{30}$$

where $P = \begin{bmatrix} \rho & \dot{\rho} & \ddot{\rho} \end{bmatrix}^T$ and matrices E, F and G are matrices obtained as a result of solving the system of linear equations in (27). The complete derivation and expression for these matrices are presented in Appendix B.

A comparison between a lane change manoeuvre done in the autonomous mode, the manual mode and the one in which a take-over is initiated by the driver is presented in Fig. 5. The time duration of interest after the switch is kept short (≈ 2.5 times the duration of the lane change) with the intention of focusing on the transient dynamics that occur after the switch.

As highlighted in the research objectives discussed in Section I, it can be seen from the plots for the lateral position (Y), lateral acceleration (a_y) and steering angle (δ) in Fig. 5 that the transients which arise due to the switch are more severe in comparison to the performance of the path tracking controller or the driver alone.

Note here that, the reference path for a lane change is defined as a fifth order polynomial function of the longitudinal position (x, measured along $\vec{e}_x^g$), as shown below :

$$y_{ref}(x) = a_0 + a_1x + a_2x^2 + a_3x^3 + a_4x^4 + a_5x^5 \tag{31}$$

where $y_{ref}(x)$ is the reference lateral position (along the direction $\vec{e}_y^g$) for the vehicle. A fifth order is chosen for the reference path because it provides six coefficient, a_0 up to a_5, that can be used to set the initial and final conditions for the reference lateral position, velocity and acceleration respectively. The reference curvature, which is the input to systems (20) and (26), can now be derived as [19] :

$$\rho(x) = \frac{d^2y/dx^2}{(1 + (dy/dx)^2)^{3/2}} \tag{32}$$

Furthermore, the input to the controller-vehicle system (26) and the driver-vehicle system (20) are parts of the same input signal, meaning that the driver 'intends' to continue the same lane change initiated by the autonomous system. This is chosen so as to eliminate the effect of in-deterministic factors such as the driver's intention from the transient dynamics that are caused purely due to a switch in control.

A detailed analysis of the transients caused due to a switch in control, is presented in the next section, along with the derivation of a performance indicator to evaluate these dynamics.

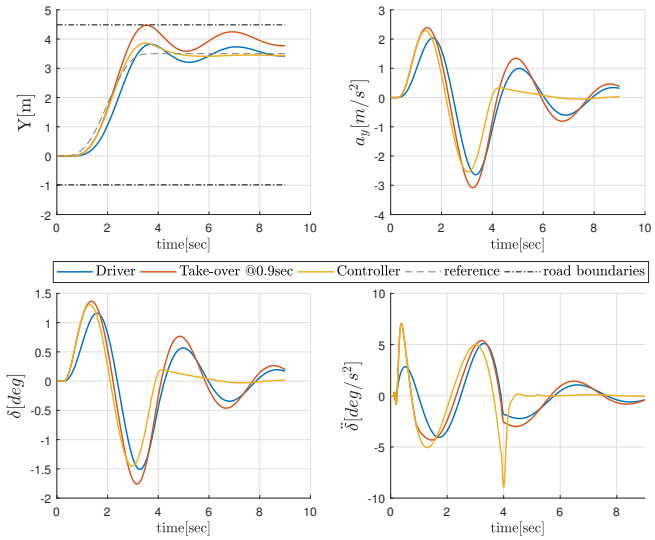

Fig. 5. Comparing a single lane change manoeuvre performed by a driver alone, path tracking controller alone and a take-over at $0.9sec$, with $v_x = 100km/h$ and lane change length L=105m, lane width =3.5m. Vehicle parameters are given in Table I, driver and controller parameters in Table II (Section IV).

III. Analysis of the Transient Dynamics

As a first step in the analysis of the transient dynamics, it is desired to obtain a 'switching performance indicator' that can be used to check if the output of interest satisfies a predefined bound. This can be useful especially for bounding states/outputs of the system that are safety critical for the application. The performance indicator is first derived for general switched linear systems, followed by a specific application to a take-over scenario.

A. Bounding the transient dynamics of switched linear systems

The general form of the switched system that is being studied in this research can be written as:

$$\dot{X}_1(t) = A_1X_1(t) + B_1u(t), \quad 0 \leq t \leq t_s \quad (33a)$$

$$\dot{X}_2(t) = A_2X_2(t) + B_2u(t), \quad t_s < t \leq T \quad (33b)$$

$$given, \; X_2(t_s) = f(X_1(t_s), u(t_s), \dot{u}(t_s), \ddot{u}(t_s)...) \quad (33c)$$

where, $X_1(t) \in \mathbb{R}^n$ and $X_2(t) \in \mathbb{R}^n$ are the state vectors, the pairs $(A_1 \in \mathbb{R}^{n\times n}, B_1 \in \mathbb{R}^n)$ and $(A_2 \in \mathbb{R}^{n\times n}, B_2 \in \mathbb{R}^n)$ are the corresponding state and input matrices of the first (33a) and second (33b) subsystems (of order n), hereafter referred to as 'System-1' and 'System-2'. The time instant of switch (t_s) is considered as an exogenous factor and the initial condition for System-2 is a given function (f) of the states of System-1, the input $(u(t) \in \mathbb{R})$ and its derivatives at the instant of switching. For an application in this research, the function f takes the form of (30). It is also to be noted here, that the System-2 is assumed to be active at least till time 'T' after the switch, which has to be large enough to include the peak transient response of the system after the switch. A specific definition of T is, however, not proposed in this research and has to be decided based on the dynamics of System-2. In addition to this, an output $(y(t))$ is defined using output matrices $C_1^T \in \mathbb{R}^n$ and $C_2^T \in \mathbb{R}^n$, given by

$$y(t) = \begin{cases} C_1X_1(t), & 0 \leq t \leq t_s \\ C_2X_2(t), & t_s < t \leq T \end{cases} \quad (34)$$

Let y_{max} be the maximum allowable absolute value of the output defined in equation (34). The required amplitude boundedness condition can be expressed as shown below:

$$\|y(t)\|_\infty \leq y_{max}, \quad t_s < t \leq T \quad (35)$$

It is to be noted here that, only the part of the output signal after the switch $(t_s < t \leq T)$ is bounded in order to isolate the transient dynamics caused by the switch. The output signal before the switch is only a function of the dynamics of System-1, its initial condition and the input, which are given and assumed to be such that the bound (35) is satisfied for $t \leq t_s$. A sufficient condition for satisfying the inequality (35), is presented in the following theorem.

Theorem 3.1: Let (33) represent the dynamics of a switched system, with each of its subsystems (33a) and (33b) being exponentially stable Linear Time Invariant (LTI) systems. Let the initial conditions of system (33b) be defined as given in (33c). The amplitude boundedness condition (35) is satisfied if:

$$\frac{y_{t_s} + \|g_2(t-t_s)\|_{\mathcal{L}_1}\|u(t)\|_\infty}{y_{max}} \leq 1, \quad t_s < t \leq T \quad (36)$$

where $g_2(t)$ is the impulse response corresponding to the output defined in (34) for $t \in (t_s, T]$ and y_{t_s} is defined as:

$$y_{t_s} := |C_1e^{A_1t_s}X_0 + C_1\int_0^{t_s} e^{A_1(t_s-\tau)}B_1u(\tau)d\tau|$$

where, X_0 is the initial condition of the system (33a).

Proof: The output $y(t)$ defined in (34) for $t \in (t_s, T]$ can be written as the solution of the system (33), given by,

$$y(t) = \underbrace{C_2 e^{A_2(t-t_s)} X_2(t_s)}_{y_1(t)} + \underbrace{C_2 \int_0^{t-t_s} e^{A_2(t-t_s-\tau)} B_2 u(\tau + t_s) d\tau}_{y_2(t)}, \quad t_s < t \leq T \tag{37}$$

where $X_2(t_s)$ is the initial condition of (33b), which can be derived using (33c). The final state of (33a) ($X_1(t_s)$) that appears in (33c) can be obtained by solving (33a) for time $t = t_s$,

$$X_1(t_s) = e^{A_1 t_s} X_0 + \int_0^{t_s} e^{A_1(t_s-\tau)} B_1 u(\tau) d\tau \tag{38}$$

In (37) $y_1(t)$ represents the zero-input response and $y_2(t)$ represents the zero-state response of system (33b) after the switch. The $\mathcal{L}_\infty$ norm of the output $y(t)$ can be written as:

$$\|y(t)\|_\infty = \|y_1(t) + y_2(t)\|_\infty, \quad t_s < t \leq T \tag{39}$$

using the triangular inequality for $\mathcal{L}_\infty$ norms,

$$\|y(t)\|_\infty \leq \|y_1(t)\|_\infty + \|y_2(t)\|_\infty, \quad t_s < t \leq T \tag{40}$$

where,

$$\|y_1(t)\|_\infty = \max_{t_s < t \leq T} |C_2 e^{A_2(t-t_s)} X_2(t_s)| \tag{41}$$

Since the subsystems of (33) are exponentially stable, all eigenvalues of A_1 and A_2 have strictly negative real parts. This means that the argument of the max function in the RHS of (41) is a decaying function, and an upper bound for $\|y_1(t)\|_\infty$ can be obtained at $t = t_s$ as,

$$\|y_1(t)\|_\infty < |C_2 X_2(t_s)| := y_{t_s} \tag{42}$$

In order to evaluate $\|y_2(t)\|_\infty$ in (40), the following Lemma is first discussed:

Lemma 3.1: [20] *If $G(s)$ is the transfer function of a system with the input signal $u(t)$, output signal $y(t)$ and $g(t)$ the impulse response matrix of $G(s)$, then for zero initial conditions, the output $y(t)$ is bounded according to:*

$$\|y(t)\|_\infty \leq \|g(t)\|_{\mathcal{L}_1} \|u(t)\|_\infty$$

Since $y_2(t)$ is the zero-state output of (33b), Lemma 3.1 can be used to bound it as:

$$\|y_2(t)\|_\infty \leq \|g_2(t-t_s)\|_{\mathcal{L}_1} \|u(t)\|_\infty, \quad t_s < t \leq T \tag{43}$$

where, $g_2(t)$ is the impulse response matrix of the transfer function from the input $u(t)$ to the output $y(t)$, which can be computed as:

$$g_2(t) = C_2 e^{A_2 t} B_2, \quad t \geq 0 \tag{44}$$

The bound on the output (40) can now be written using (42) and (43) as:

$$\|y(t)\|_\infty \leq y_{t_s} + \|g_2(t-t_s)\|_{\mathcal{L}_1} \|u(t)\|_\infty, \quad t_s < t \leq T \tag{45}$$

A sufficient condition for satisfying the upper bound on the output defined in (35) can now be formulated using (45) as:

$$\frac{y_{t_s} + \|g_2(t-t_s)\|_{\mathcal{L}_1} \|u(t)\|_\infty}{y_{max}} \leq 1, \quad t_s < t \leq T$$

■

B. Discussion

The sufficient condition derived in Theorem 3.1 can be seen as a switching performance indicator, for satisfying bounds on the output of the form (35). By definition, the indicator focuses on the transient time period after a switch and is applicable for a general input ($u(t)$). It is also to be noted that by using the triangle inequality for the $\mathcal{L}_\infty$ norms in (40) and subsequently using Lemma 3.1 for bounding $\|y_2(t)\|_\infty$, a considerable level of conservativeness is introduced in the final bound that is obtained. The level of conservativeness is discussed in Section IV by comparing it with simulation results.

This result can now be applied to the specific case of a take-over scenario using the models developed in Section II, as it will be discussed in the next part of this section.

C. Bounding the transient dynamics of a take-over

The closed-loop dynamics for a take-over can be summarized from the dynamics derived in Section II as shown below:

$$\dot{X}_c(t) = A_{cc} X_c(t) + B_{cc} \rho(t), \quad 0 \leq t \leq \tau_{to} \tag{46a}$$

$$\dot{X}_d(t) = A_{dc} X_d(t) + B_{dc} \rho(t), \quad \tau_{to} < t \leq t_{tr} \tag{46b}$$

$$given,\ X_d(\tau_{to}) = E^{-1}(F X_c(\tau_{to}) + G P(\tau_{to})) \tag{46c}$$

where t_{tr} is the end of the transient period that is chosen for the analysis. The outputs of interest are defined on the system using output matrices C_{cc} and C_{dc} given by,

$$y(t) = \begin{cases} C_{cc} X_c(t), & 0 \leq t \leq \tau_{to} \\ C_{dc} X_d(t), & \tau_{to} < t \leq t_{tr} \end{cases} \tag{47}$$

Theorem 3.1 when applied to the system description (46), for output (47), gives a sufficient condition for satisfying a bound of the form (35) as given below:

$$G_1 := \frac{y_{\tau_{to}} + \|g_d(t-\tau_{to})\|_{\mathcal{L}_1} \|\rho(t)\|_\infty}{y_{max}} \leq 1, \quad \tau_{to} < t \leq t_{tr} \tag{48}$$

where,

$$y_{\tau_{to}} = |C_{cc} e^{A_{cc}\tau_{to}} X_{c_0} + C_{cc} \int_0^{\tau_{to}} e^{A_{cc}(\tau_{to}-\tau)} B_{cc} \rho(\tau) d\tau|$$

with X_{c_0} the initial condition of system (46a) and $g_d(t)$ the impulse response corresponding to the output (47) for

the driver-vehicle system (46b).

A simpler representation of G_1 (48) can be obtained by using some properties of the system (46) and the input $\rho(t)$ (for specific driving manoeuvres). This is done in the following parts of this section, by first expressing the 'finite time $\mathcal{L}_1$ norm' of the impulse response (that appear in (48)) using the eigenvalues of the system, followed by approximating the input signal as a sinusoid for a lane change manoeuvre.

1) A Growth relationship for finite time $\mathcal{L}_1$ norms: The $\mathcal{L}_1$ norm of the impulse response $g_d(t)$ that appears in (48) is to be computed over a finite time period ($\tau_{to} < t \leq t_{tr}$) which can alternatively be represented in terms of the eigenvalues of the state matrix (A_{dc}). This is done by taking advantage of the fact that the state matrices of the closed-loop dynamics in (46) are Hurwitz (known from the models developed in Section II).

The impulse response $g_d(t)$ can be computed from the state space matrices as shown below:

$$g_d(t) = C_{dc} e^{A_{dc} t} B_{dc} \tag{49}$$

As A_{dc} is Hurwitz, there exist positive constants c and λ such that the impulse response can be bounded as shown below [21]:

$$|g_d(t)| \leq c e^{-\lambda t} \tag{50}$$

Moreover, since all eigenvalues of A_{dc} have multiplicity equal to 1, λ can be chosen as the absolute value of the largest (least negative) real part of the eigenvalues [21]. Finding c analytically for the upper bound (50) to be tight is challenging, given the complexity in the structure of $g_d(t)$ (due the high order (8^{th}) of the state space). However, a work around is proposed here, using the absolute maximum of the impulse response ($\|g_d(t)\|_\infty$). First, the time (t_∞) at which the absolute maximum value is attained by the impulse response is defined as:

$$t_\infty = \{t \mid \quad |g_d(t)| = \|g_d(t)\|_\infty,\ t \geq 0\} \tag{51}$$

an approximate lower bound on c can be formulated using (50) and (51) as:

$$\begin{aligned} \|g_d(t)\|_\infty = |g_d(t_\infty)| \leq c e^{-\lambda t_\infty} \\ c \geq \|g_d(t)\|_\infty e^{\lambda t_\infty} \end{aligned} \tag{52}$$

A word of caution has to be made here regarding using the lower bound obtained in (52), as it is a necessary but not a sufficient condition for satisfying (50). It can however, be seen as a reasonable initial estimate to obtain an optimal value for c, that does not make the RHS of (50) a conservative bound on $|g_d(t)|$.

An illustration of the bound (50) for the impulse response of the lateral tracking error of the vehicle (y_e) is presented in Fig. 6 with the value of c set at its minimum value obtained in (52). In this example, $g_d(t)$ is computed using the vehicle parameters in Table I and driver model parameters in Table II, with the values for c and λ obtained as 341.24 and 0.0639 respectively.

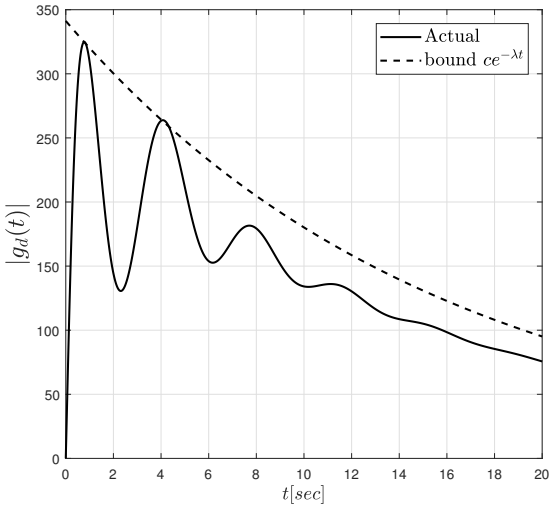

Fig. 6. Comparing $|g_d(t)|$ with the bound (50) and c equal to the lower bound in (52), for output chosen as the lateral tracking error y_e. Here, $c = 341.24$ and $\lambda = 0.0639$.

The finite time $\mathcal{L}_1$ norm can be computed using the bound in (50), as shown below:

$$\begin{aligned} \int_0^\tau |g_d(t)| dt &= \int_0^\tau |C_{dc} e^{A_{dc} t} B_{dc}| dt \\ &\leq c \int_0^\tau e^{-\lambda t} dt \\ &= \frac{c}{\lambda}(1 - e^{-\lambda \tau}) \end{aligned} \tag{53}$$

where τ is the time up to which the $\mathcal{L}_1$ norm is to be computed. The final expression obtained in (53) can be seen as a growth relationship that bounds the finite time $\mathcal{L}_1$ norm, as it grows with τ at an exponential rate governed by λ. A comparison between this relation and the actual value of the $\mathcal{L}_1$ norm is presented in Fig.7, for the output chosen as the lateral position error (y_e). It can be seen that the bound is satisfied but gets increasingly conservative for larger values of τ. However, by virtue of the simplicity that the relation offers, it deserves to be used as a substitute for the actual norms in (48) for obtaining a more intuitive sufficient condition for bounding the output amplitude, given by:

$$G_2 := \frac{y_{\tau_{to}} + \frac{c}{\lambda}(1 - e^{-\lambda(t_{tr} - \tau_{to})}) \|\rho(t)\|_\infty}{y_{max}} \leq 1, \qquad \tau_{to} < t \leq t_{tr} \tag{54}$$

Note here that (54) is obtained by substituting τ as the transient time period ($t_{tr} - \tau_{to}$) in (53) and subsequently

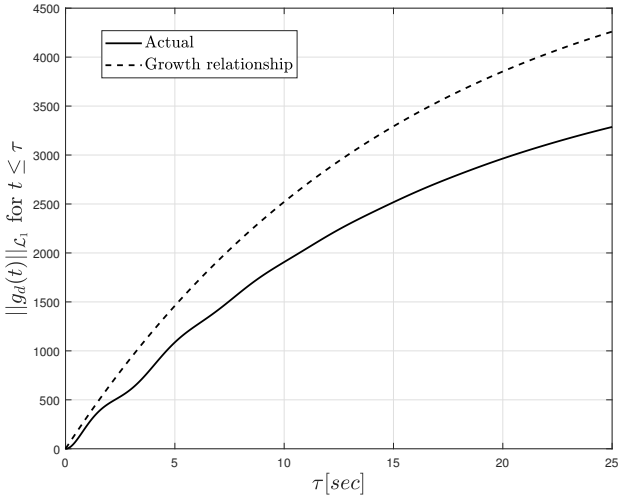

Fig. 7. Comparison of the growth relationship (53) with the actual value of the finite time $\mathcal{L}_1$ norm of $g_d(t)$, for output chosen as the lateral position error (y_e). Here, $c = 341.24$ and $\lambda = 0.0639$.

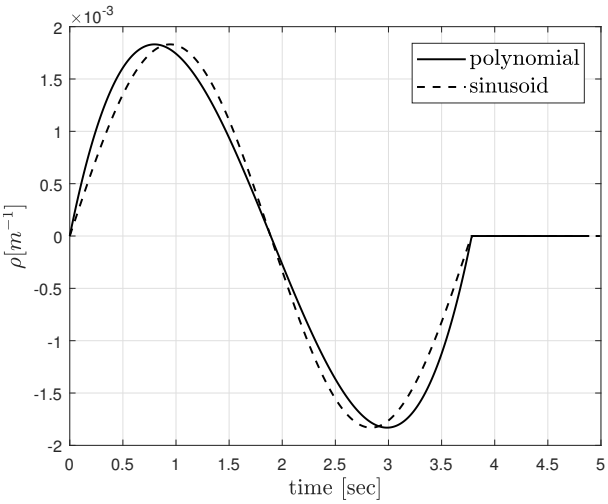

Fig. 8. Comparison between the sinusoidal approximation (55) with the actual polynomial curvature (32), for a single lane change of $t_{lc} = 3.8sec$, $v_x = 100km/h$, lane width = 3.5m

using it in the place of $\|g_d(t - \tau_{to})\|_{\mathcal{L}_1}$ in (48). Although a simpler expression for the sufficient condition is obtained in (54), it is more conservative than (48) due to the fact that a bound on the finite time $\mathcal{L}_1$ norm is used in the place of its actual value. The level of conservativeness introduced in (54) will be discussed in Section IV.

The next part of this section discusses how the results obtained in this section can be used along with the properties of the input ($\rho(t)$) for a lane change manoeuvre to obtain a similar bound on the output.

2) Bounding the transients of a lane change manoeuvre: The input to the system represented by (46) is the curvature of the reference trajectory, which can be approximated as a low frequency sinusoid ($0.2 - 0.4Hz$ in this study) for a single lane change manoeuvre. The input can thus be written as:

$$\rho(t) = \begin{cases} A_\rho sin(\omega t) & 0 \leq t \leq t_{lc} \\ 0 & t > t_{lc} \end{cases} \tag{55}$$

where A_ρ and ω are the amplitude, frequency of the sinusoid. The time taken for the lane change (t_{lc}) is also the time period of the sinusoid and hence, $\omega := 2\pi/t_{lc}$. A comparison between the sinusoidal approximation (55) with the actual polynomial curvature (32) for a single lane change manoeuvre, is done in Fig. 8.

The output signal (47) after the take-over ($\tau_{to} < t \leq t_{tr}$) can be written as the sum of the zero-input and zero-state responses, of which the zero-state response can be written as a convolution integral of the input with the impulse response $g_d(t)$, as shown below:

$$|y(t)| = \begin{cases} |C_{dc}e^{A_{dc}(t-\tau_{to})}X_d(\tau_{to}) + \int_0^{t-\tau_{to}} g_d(t - \tau_{to} - \tau)\rho(\tau + \tau_{to})d\tau|, & \tau_{to} < t \leq t_{lc}, \\ |C_{dc}e^{A_{dc}(t-\tau_{to})}X_d(\tau_{to}) + \int_0^{t_{lc}-\tau_{to}} g_d(t - \tau_{to} - \tau)\rho(\tau + \tau_{to})d\tau|, & t_{lc} < t \leq t_{tr} \end{cases} \tag{56}$$

Here, the output is derived in two parts due to a similar definition of the input (55), separated at $t = t_{lc}$. It is to be noted that the only difference between the two separate parts of the output is in the upper limit of the convolution integral, being limited to $(t_{lc} - \tau_{to})$ for $t > t_{lc}$ as the input is 0 during this time period.

A bound on the output can now be derived by substituting the bound on the impulse response (50) in the place of the actual impulse response $g_d(t)$ in (56) which on evaluation gives:

$$|y(t)| \leq \begin{cases} |C_{dc}e^{A_{dc}(t-\tau_{to})}X_d(\tau_{to}) + \\ A_\rho c\{\sin(\omega t - \theta) + e^{-\lambda(t-\tau_{to})}\sin(\theta - \phi)\}|, & \tau_{to} < t \leq t_{lc} \\ |C_{dc}e^{A_{dc}(t-\tau_{to})}X_d(\tau_{to}) + \\ A_\rho c\{e^{-\lambda(t-\tau_{to})}\sin(\theta - \phi) - e^{-\lambda(t-t_{lc})}\sin\theta\}|, & t_{lc} < t \leq t_{tr} \end{cases}$$
$$:= \zeta(t), \quad t \in (\tau_{to}, t_{tr}] \tag{57}$$

where, $\theta = \arctan(\frac{\omega}{\lambda})$, $\phi = \omega\tau_{to}$ and $\omega = \frac{2\pi}{t_{lc}}$

An absolute bound over the output ($\|y(t)\|_\infty$) can be found by evaluating the RHS of (57) ($\zeta(t)$) and taking

the maximum over $t \in (\tau_{to}, t_{tr}]$. A sufficient condition for satisfying output bounds of the form (35) can then be defined as,

$$G_3 := \max_{t\in(\tau_{to},t_{tr}]} \frac{\zeta(t)}{y_{max}} \leq 1 \tag{58}$$

An illustration of this absolute bound is presented in the next section by comparing it with the bounds obtained in (48), (54) and through simulations. An illustration of how these bounds (or performance indicators) can be used to obtain safe regions on a specific parameter space is also discussed in the next section.

IV. Simulations and Validation

Using the models developed in Section II, simulations are performed to obtain the peak values of the transients in the states/outputs after a switch. The simulations are performed for a single lane change manoeuvre as discussed in Section II-E. Two independent factors are identified that can be varied, to generate different take-over conditions:

- Length of the lane change (L) - is a measure of the severity of the manoeuvre initiated by the autonomous system. A shorter lane change is more severe for the same forward velocity (v_x) of the vehicle.
- Time of take-over (τ_{to}) - as already discussed, this is the parameter that defines the time instant at which the control switches from the autonomous system to the driver.

These two parameters are selected in order to study the effect of the input trajectory and the switching parameter on the transient lateral dynamics of the vehicle (for a given driver, vehicle and path tracking controller). Note that the input to the system for the lane change manoeuvre is the reference curvature defined in (32).

For the purpose of illustration, the lateral acceleration of the vehicle ($a_y[m/s^2]$) is chosen as the output of interest and its maximum allowable absolute value ($a_{y_{max}}$) is set as $4m/s^2$. The parameter values of the driver model and the path tracking controller, are summarized in Table II .

TABLE II
Driver and Path Tracking Controller Parameters (Appendix A, C)

Driver Parameter	Value	Controller parameter	Value
k	0.24	ω_0[rad/s]	17.5
$T_L[sec]$	16	β_{str}[Nm sec/rad]	0.7
$\tau_d[sec]$	0.099	τ_{str}[sec]	0.1
$T_I[sec]$	0.91	k_1	0.008
$T_N[sec]$	0.47	k_2	0.339
k_e	0.0071	k_{ff}	0.274
l_a	14.08		
k_r	0.08		

The peak absolute value of the output (here a_y) is first obtained through simulations by numerically solving the dynamics of the system (46) which is then compared with the bounds G_1 (48), G_2 (54) and G_3 (58), as shown in Fig. 9. It can be seen that the bound G_1 is the least

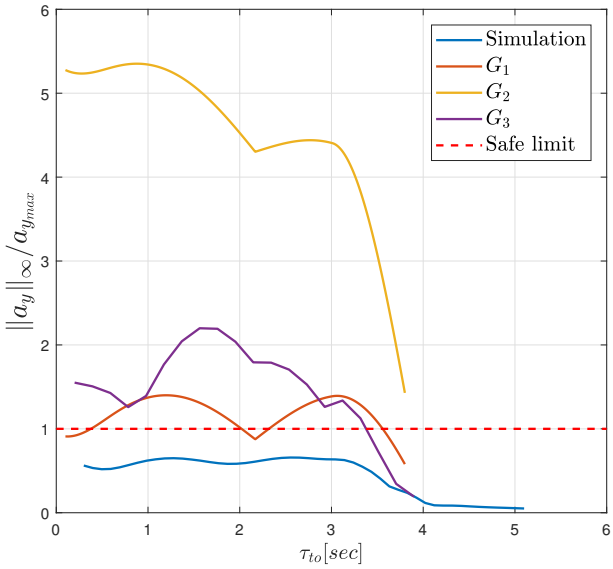

Fig. 9. Comparison of G_1, G_2 and G_3 with simulations for a constant $L = 105m$, $\tau_{to} = [0.1...3.9]sec$ and $a_{y_{max}} = 4m/s^2$. The safe limit is indicated by the red dashed line.

conservative followed by G_3 and G_2. This is due to the fact that G_1 is derived using the actual impulse response function making it less conservative in comparison to G_3 and G_2, which use the bound on the impulse response (50). Having a simpler representation (G_2 and G_3) in terms of the eigenvalues of the system has thus resulted in an increase in the conservativeness. Furthermore, using a more precise definition of the input signal has helped in reducing the conservativeness from G_2 to G_3. Overall, it can be said that G_1 provides a bound that is least conservative and most generic at the same time.

The bound G_1 is now compared with the simulations for a range of values for L and τ_{to} as shown in Fig. 10. It can be seen that G_1 bounds the absolute peak of the transients obtained through simulations for the entire range of parameters, although it is still conservative to some degree. The safe level for the bound is indicated by a plane at a value of 1 (indicated in blue, in Fig. 9). The portions of the surfaces that have a value greater than 1 can be projected on to the L vs τ_{to} plane, resulting in a classification of the parameter space into safe and unsafe regions, as illustrated in Fig. 11. Although using the bound G_1 demarcates a larger area as unsafe in the parameter space, it does follow the trend seen in the simulations that a smaller value of L (faster lane change) is more severe to a take-over and that for a given value of L some values of τ_{to} can be more critical.

The bounds developed in this research can thus be used as performance indicators for the transient dynamics which

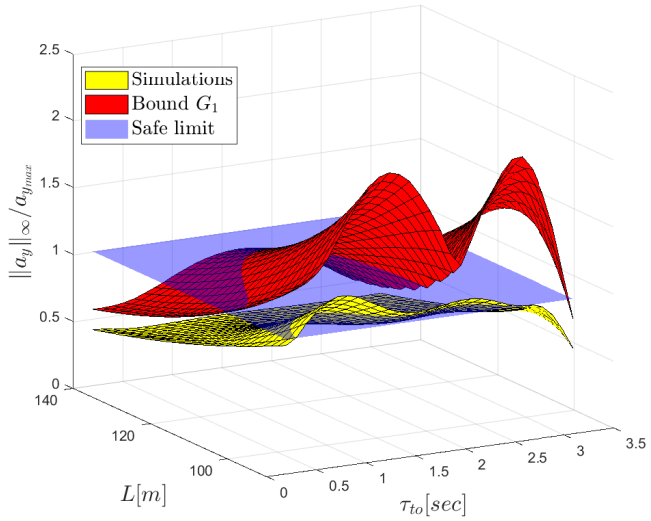

Fig. 10. Illustration of the absolute bound on $a_y(t)$ obtained from G_1 (48) with respect to simulation results, for $L = [90...140]m$ and $\tau_{to} = [0.1...3.5]sec$

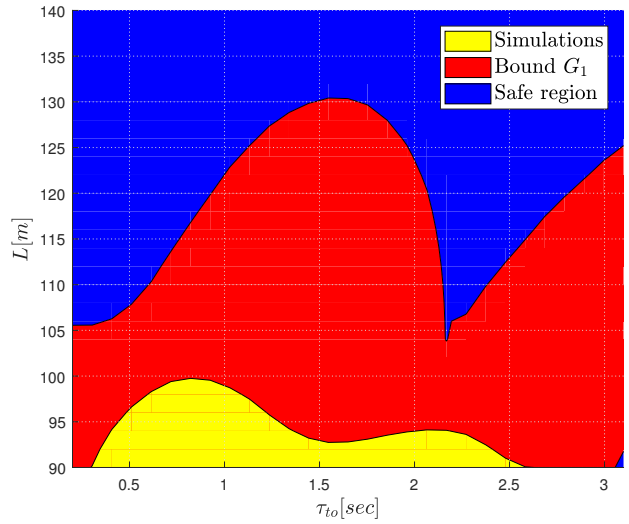

Fig. 11. Safe and unsafe regions in the parameter space $L[m]$ vs $\tau_{to}[sec]$, obtained by projecting the portions of the bounds in Fig. 10 that have a value greater than 1, on to the $L[m]$ vs $\tau_{to}[sec]$ plane

in turn classifies parameter spaces into safe/unsafe regions similar to Fig. 11.

V. Conclusions and Recommendations

A. Conclusions

This research has put forth a switching performance indicator that can be used to evaluate the level of safety during a driver initiated take-over from an autonomous driving system. The driver and the vehicle are modeled as LTI systems and a path tracking controller is used to serve as an autonomous driving system. The take-over is then studied as a switch from the path tracking controller to the driver. The safety of a take-over is evaluated based on whether an output of interest satisfies a predefined absolute bound, after the take-over. This is done by first, deriving a sufficient condition that can guarantee an absolute bound on the output after a switch, followed by obtaining a representation of the sufficient condition in terms of the eigenvalues of the system and the properties of the input signal. These sufficient conditions or bounds can also be interpreted as switching performance indicators as they can be used to pre-determine the safety of a take-over based on the structure and settings of the system components (driver, vehicle and path tracking controller).

Finally, a comparison is made between the bounds obtained through simulations and the one obtained by evaluating the sufficient conditions. It has been found that the bounds given by the sufficient conditions captures the trend seen in the simulation results to some extent, as a function of two parameters that define the input signal and the switching time instant respectively. Even though the level of conservativeness in these bounds make them difficult to be used directly in real applications, they are useful for an initial estimation of a bound on the transient dynamics while designing systems that involve shared or multi-modal control, without having to perform extensive simulations.

It is also observed that reducing the conservativeness of such an approach is a challenge beyond what is achieved here.

B. Recommendations for future work

In this research, the performance or safety of a switch is evaluated only in terms of bounding the absolute peak value of the states/outputs, which is not sufficient to completely quantify the transient dynamics arising due to a switch. The frequency content of the transients can also be a major concern for safety, which can be studied, for e.g. using the induced $\mathcal{L}_2$ norms as done in [9] or the Root-mean-square gains as proposed in [22].

An investigation on developing a unified indicator that combines different properties of the transients and a quantitative measure of its conservativeness are some steps that can be taken towards making such an approach useful in real world applications.

Further research is necessary in determining how such performance indicators can be effectively used in the design of semi/multi-modal autonomous driving systems.

References

[1] D. T. McRuer, R. W. Allen, D. H. Weir, and R. H. Klein, "New results in driver steering control models," *Human factors*, vol. 19, no. 4, pp. 381–397, 1977.

[2] J. Craens and N. Das., "taking over the steering of a toyota prius using the electric steering motor," *Technical report, Fontys*, 2014.

[3] M. Bertoncello and D. Wee, "Ten ways autonomous driving could redefine the automotive world," *Mckinsey and company*, vol. 50, no. 15, 2015.

[4] D. Kohler and A. Brotschi, "Automotive revolution perspective towards 2030," *Advanced Industries, Mckinsey and company*, 2016.

[5] Z. Lu, R. Happee, C. D. Cabrall, M. Kyriakidis, and J. C. de Winter, "Human factors of transitions in automated driving: A general framework and literature survey," *Transportation Research Part F: Traffic Psychology and Behaviour*, vol. 43, pp. 183 – 198, 2016.

[6] W. P. Vlakveld, "Transition of control in highly automated vehicles: a literature review," *SWOV Institute for Road Safety Research, The Hague*, pp. 30 p., 38 ref.; R–2015–22, 2016.

[7] C. Gold, D. Dambck, L. Lorenz, and K. Bengler, "take over! how long does it take to get the driver back into the loop?," *Proceedings of the Human Factors and Ergonomics Society Annual Meeting*, vol. 57, no. 1, pp. 1938–1942, 2013.

[8] N. Merat, A. H. Jamson, F. C. Lai, M. Daly, and O. M. Carsten, "Transition to manual: Driver behaviour when resuming control from a highly automated vehicle," *Transportation Research Part F: Traffic Psychology and Behaviour*, vol. 27, pp. 274 – 282, 2014.

[9] J. Ploeg, N. Van De Wouw, and H. Nijmeijer, "Lp string stability of cascaded systems: Application to vehicle platooning," *IEEE Transactions on Control Systems Technology*, vol. 22, no. 2, pp. 786–793, 2014.

[10] S. Boyd, L. El Ghaoui, E. Feron, and V. Balakrishnan, *Linear matrix inequalities in system and control theory*, vol. 15. Siam, 1994.

[11] J. P. Hespanha and A. S. Morse, "Stability of switched systems with average dwell-time," in *Decision and Control, 1999. Proceedings of the 38th IEEE Conference on*, vol. 3, pp. 2655–2660, IEEE, 1999.

[12] M. Kaustubh, D. Willemsen, and M. Mazo, "The modeling of transfer of steering between automated vehicle and human driver using hybrid control framework," in *Intelligent Vehicles Symposium (IV), 2016 IEEE*, pp. 808–814, IEEE, 2016.

[13] H. Pacejka, *Tire and vehicle dynamics*. Elsevier, 2005.

[14] A. Schmeitz, J. Zegers, J. Ploeg, and M. Alirezaei, "Towards a generic lateral control concept for cooperative automated driving theoretical and experimental evaluation," in *Models and Technologies for Intelligent Transportation Systems (MT-ITS), 2017 5th IEEE International Conference on*, pp. 134–139, IEEE, 2017.

[15] T. Jürgensohn, "Control theory models of the driver," *Modelling driver behaviour in automotive environments*, pp. 277–292, 2007.

[16] A. Modjtahedzadeh and R. A. Hess, "A model of driver steering control behavior for use in assessing vehicle handling qualities," *Transactions-american society of mechanical engineers journal of dynamic systems measurement and control*, vol. 115, pp. 456–456, 1993.

[17] D. T. McRuer and E. S. Krendel, "Mathematical models of human pilot behavior," tech. rep., Advisory group for aerospace research and development Neuilly-sur-seine (France), 1974.

[18] J. C. Gerdes and E. J. Rossetter, "A unified approach to driver assistance systems based on artificial potential fields," *Transactions-american society of mechanical engineers journal of dynamic systems measurement and control*, vol. 123, no. 3, pp. 431–438, 2001.

[19] R. Rajamani, *Vehicle dynamics and control*. Springer Science & Business Media, 2011.

[20] C. A. Desoer and M. Vidyasagar, *Feedback systems: input-output properties*, vol. 55. Siam, 1975.

[21] J. P. Hespanha, *Linear systems theory*. Princeton university press, 2009.

[22] J. P. Hespanha, "Root-mean-square gains of switched linear systems," *IEEE Transactions on Automatic Control*, vol. 48, no. 11, pp. 2040–2045, 2003.

NOMENCLATURE

Acronyms and abbreviations

DI	Driver Initiated
D2V	Driver to Vehicle
LMI	Linear Matrix inequality
RMS	Root Mean Squared
VI	Vehicle Initiated
V2D	Vehicle to Driver

Roman symbols

$a_0 ... a_5$	Reference path coefficients
a_y	Lateral acceleration
A_ρ	Amplitude of approx. sinusoidal input
C	Tyre cornering stiffness (see general subscripts)
$C_{\Delta_d}, C_{\Delta_c}$	Output matrices for δ_d,δ_c
f	Function defining initial conditions for System 2
F	Force
g	Impulse response matrix
g_1, g_2	Impulse responses, general systems 1,2
G_1, G_2,G_3	Bounds on the transient dynamics
I_{zz}	Moment of inertia about Z-axis
k	Gain - operator model
k_e	Feedback gain - driver
k_r	Feedforward gain - driver
k_1, k_2	Feedback gains - controller
k_{ff}	Feedforward gain - controller
K_c	Feedback gain matrix - controller
K_d	Feedback gain matrix - driver
K_δ	Understeer coefficient
l_a	Look ahead distance
l	Wheelbase
L	Length of lane change
m	Mass of the vehicle
$\mathcal{O}$	Reference point
R	Direction cosine matrix
t_s	General system, switching time instant
T	General system, transient time period
T_L	Lead time constant - human operator
T_I	Lag time constant - human operator
T_N	Neuromuscular time constant
t_{tr}	Transient time period
t_{lc}	Lane change time
t_s	Switching time instant - general system
u	General input
v	Velocity
X_1, X_2	State vectors - General system 1,2
X	State vector
X_0	Initial state vector
y	Lateral position
A, B, C	State space matrices (see general subscripts)
E,F,G,P	Matrices for state transformation

Greek symbols

α	Lateral slip angle of the tyre
β	Heading angle
β_{str}	Steering actuator damping coefficient
δ	Steering angle
$\delta_{d_1} ... \delta_{d_4}$	Dummy variables - driver dynamics
$\delta_{c_1} ... \delta_{c_4}$	Dummy variables - steering actuator dynamics
Δ	Vector of dummy variables
λ	Least negative eigenvalue
ω	Frequency of the approx. sinusoidal input
ω_0	Steering actuator natural frequency
ω_z	Yaw velocity
ϕ	phase angle
ψ	Heading angle

θ_s	Orientation of the reference path at point s
ρ	Curvature of reference path
τ_{to}	Take-over time instant
τ_d	delay - driver dynamics
τ_{str}	delay - steering actuator
ζ	analytic expression for the output signal

General subscripts

x	longitudinal direction
y	lateral direction
f	front axle
r	rear axle
e	error
d	driver
c	path tracking controller
des	driver desired
set	set point
str	steering
cc	controller-vehicle closed loop
dc	driver-vehicle closed loop
max	maximum allowable value
fb	Feedback
ff	Feedforward
$1, 2$	General systems 1,2 (for state matrices)

General Superscripts

i	vehicle fixed
g	ground fixed
s	moving point on the path

Miscellaneous

$\vec{e}$	unit vector
$\vec{r}$	position vector
$\underline{\vec{e}}$	reference frame
$\|.\|_\infty$	$\mathcal{L}_\infty$ norm
$\|.\|_{\mathcal{L}_1}$	$\mathcal{L}_1$ norm

APPENDIX A
THE DRIVER MODEL

The driver's control inputs to the vehicle after a take-over are crucial for a safe transition of control. There exists a number of attempts in literature to study the driver's behaviour after a take-over [7] [8]. This appendix discusses how these characteristics in driver behaviour can be modeled within the framework of linear control systems.

A. Driver models using control theory

The driver models developed by various scientists in the 20^{th} century, are put together in [15], the most widely used among them being the multi-modal control structure developed by [1]. Most of the work on driver modeling in the late 20^{th} and the 21^{st} century are along the same lines as [1].

According to [1], the driver's control actions can be classified into three modes, namely Compensatory control, Pursuit control and Precognitive control, as shown in Fig. A.1. The compensatory control actions are those inputs from the driver during a normal lane regulation task. This could be in response to an error in the heading or lateral position of the vehicle from the reference lane. The pursuit control is the driver's effort to improve the path following, which can also be described as a feed-forward of the road curvature. The precognitive control is a set of learned and patterned open loop responses by the driver in a known driving scenario. It should be noted that these three modes of the driver are almost never present simultaneously, but are useful in describing driver behaviour during different scenarios as listed in Table A.1.

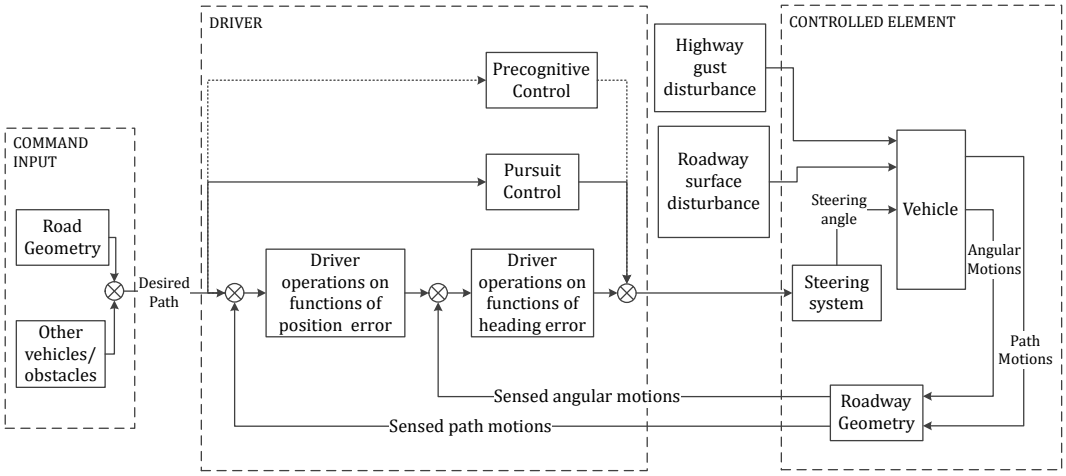

Fig. A.1. Topology of the driver-vehicle system combining open and closed-loop, precognitive, pursuit and compensatory control structures [1]

TABLE A.1
DRIVING TASKS MAPPED TO DRIVER CONTROL MODES [1]

Task or manoeuvre	**Driver Control Mode**
Normal lane regulation	Compensatory
Precision course control	Pursuit
Turns, merges. drops. and exits	Pursuit
Lane change	Dual mode (precognitive-compensatory or pursuit-compensatory)
Overtaking and passing	Dual mode (precognitive-pursuit)
Emergency lane change or evasive manoeuvre	Dual mode (precognitive-compensatory)

It can also be seen from Table A.1 that for lane change manoeuvres (which is the use case chosen in this research for studying a take-over) the Pursuit-compensatory control mode is most suitable. This control structure can be represented using the block diagram in Fig. A.2, in which the feedback component corresponds to the compensatory control while the feedforward component corresponds to the pursuit control mode. The signals and gains in Fig. A.2 are explained in Table A.2.

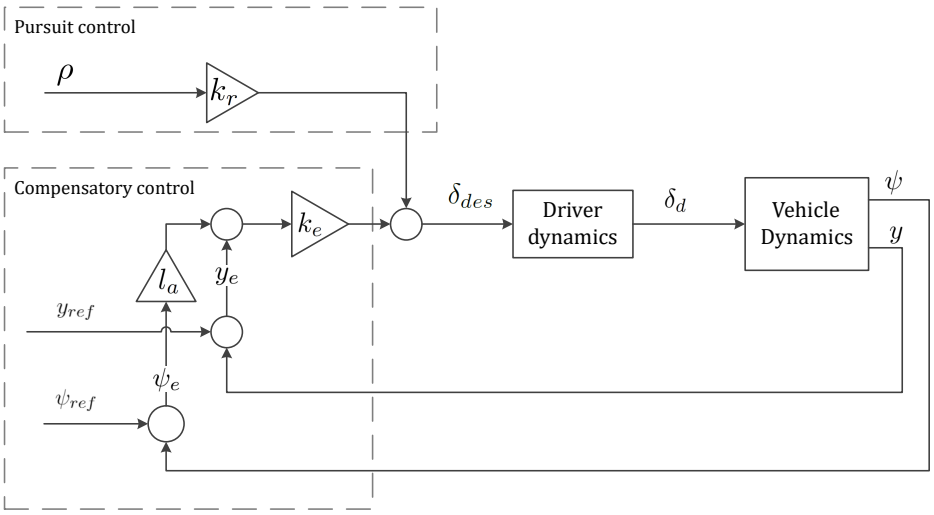

Fig. A.2. Pursuit-Compensatory control mode

TABLE A.2
SIGNALS AND GAINS IN FIG. A.2

Signal/Gain	Description
y	Global Y co-ordinate of the vehicle
ψ	Heading angle of the vehicle
y_e	Tracking error in the lateral position y
ψ_e	Tracking error in the heading angle ψ
y_{ref}	Global Y co-ordinate of the reference path
ψ_{ref}	Reference heading angle of the
δ_{des}	Driver desired steering angle
δ_d	Realised steering angle
ρ	Curvature of the reference path
k_r	Feedforward (Pursuit) gain
k_e, l_a	Feedback (compensatory) gains

Moreover, δ_{des} can be written as:

$$\delta_{des} = k_e(y_e + l_a\psi_e) + k_r\rho \tag{A.1}$$

where, k_e and k_r can be used to tune the driving behaviour towards the pursuit or the compensatory side. The term $(y_e + l_a\psi_e)$ in (A.1) is the effective tracking error that is perceived by the driver, due to the error in the lateral position and the heading angle. This effective error can also be interpreted as the error in the lateral position of a point that is ahead of the vehicle by a distance of l_a metres. The term $k_r\rho$ is the feed forward component of the driver's desired steering input due to the curvature of the road.

Furthermore, the gains k_e, k_r and the preview length l_a in (A.1) were identified in [1] using experimental data from a driving simulator. The experiment was done with 6 drivers, driving in a simulated curvy road with wind disturbances. These values are summarized in Table A.3.

TABLE A.3
GAINS k_e, l_a AND k_r IN EQUATION (A.1) [1]

Parameter	$k_e[rad/m]$	$1/l_a[m]$	k_r
Compensatory (Wind Gust Regulation) 24 total runs on six subjects			
Mean	0.014	0.072	0
σ	0.0012	0.026	0
Pursuit (Curved Path Following) 22 total runs on six subjects			
Mean	0.0221	0.127	0.054
σ	0.0054	0.095	0.02

B. Driver operator model

The quantity δ_{des} is the driver's desired steering angle which is realized based on the driver's physiological capabilities. These physiological properties of the driver, represented by the block 'Driver dynamics' in Fig. A.2 are modeled using 'human operator models' from literature, summarized in [16].

A parametric model that provides the flexibility of modifying different properties of the driver, whilst fitting in a linear control framework is proposed in [17], called the 'Quasi-linear model'. The model describes the human operator by means of a linear second-order transfer function ($H(s)$) with a dead time, given by,

$$H(s) = \frac{\delta_d}{\delta_{des}} = \frac{k(T_L s + 1)}{(T_I s + 1)(T_N s + 1)} e^{-\tau_d s} \tag{A.2}$$

The input to this model is δ_{des} and the output from the model is the actual steering angle (δ_d) achieved by the driver. Differences in the task environment and in operator properties are described by means of five independent parameters. τ_d is the reaction time of the driver in response to a change in the reference path. It can be considered as the time needed to perceive and process the control input necessary. T_N is the time constant of the neuromuscular dynamics, which is the time required for the muscles in the drivers arms to receive and execute the actions from the central nervous system. T_L and T_I are time constants of the lead lag filter which depend on how well the driver is accustomed to the vehicle or knows a certain route. k is the driver gain which could be influenced by numerous factors like the driver's driving style, urgency, level of attention etc. The Quasi-linear model in (A.2) is not a fixed model for the driver but a parametric approximation of driver behaviour, with the parameters themselves varying depending on the type of driver, vehicle and the driving scenario, which explains the prefix 'Quasi' in the nomenclature of the model. This model is also widely accepted in literature and used by a number of studies to human driving behaviour in different driving conditions [18].

Although the parameters in (A.2) are variable depending on the driving situation, it was observed in [1] that the combined driver-vehicle open loop transfer function ($H(s)G_{\psi\delta}(s)$), from δ_{des} to ψ, is invariant around the crossover frequency (here, $G_{\psi\delta}(s)$ is the transfer function describing the vehicle's yaw angle response to a steering input). According to [1] this open loop transfer function can be approximated by an integrator and an additional phase correction using a dead time for all task environments in the region of the crossover frequency (ω_c), as given by the transfer function,

$$L(s) = \frac{\omega_c}{s} e^{-\tau_d s} \tag{A.3}$$

This model is widely refered to as the 'Driver-vehicle crossover model' in literature.

The crossover frequency has been experimentally found in [16] to lie between 1.5 and 5 rad/s for most passenger cars at speeds ranging from 50 to 100 km/h . Although the exact crossover frequency is not known, this range can be used for identifying the parameters in the operator model (A.2). This is done by first choosing a nominal set of parameters such that the open loop system ($H(s)G_{\psi\delta}(s)$) is consistent with the crossover model ($L(s)$) for a nominal cross over frequency of around 3 rad/s, followed by determining a range of values for the parameters, such that the crossover frequency lies between 1.5 and 5 rad/s. This is illustrated in Fig. A.3, with the parameter ranges (which can be regarded as uncertainties here) given in Table A.4. Note here, that the transfer function $G_{\psi\delta}(s)$, is computed using the vehicle specifications given in Table I (Section II-B).

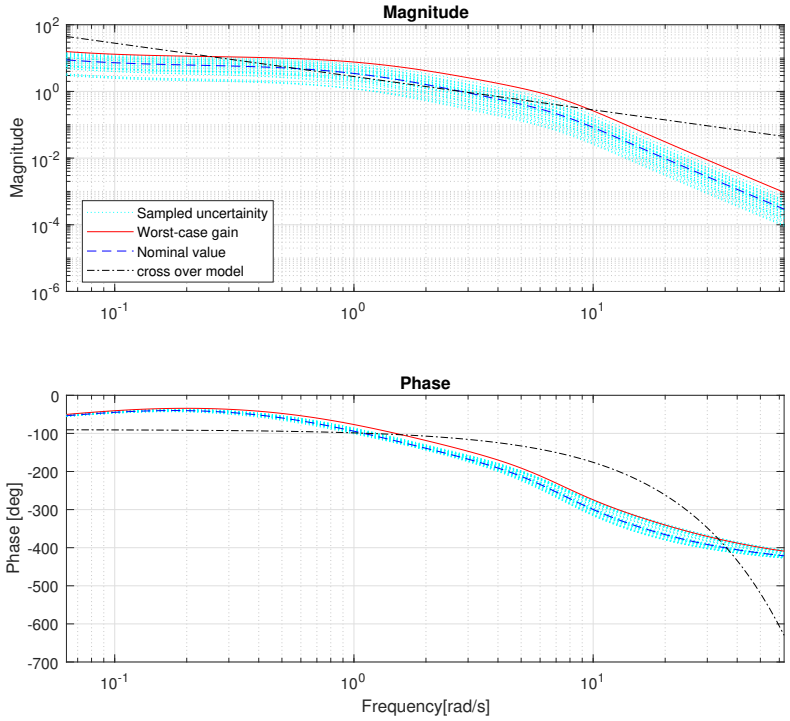

Fig. A.3. Effect of parameter uncertainties in the driver model

TABLE A.4
DRIVER MODEL PARAMETERS AND UNCERTAINTIES

Driver Parameter	Nominal value	Uncertainty range
k	0.14	± 0.1
$T_L[sec]$	15	± 1
$\tau_d[sec]$	0.15	± 0.06
$T_I[sec]$	1.11	± 0.2
$T_N[sec]$	0.67	± 0.2

APPENDIX B
CONDITIONS FOR CONTINUITY WHILE SWITCHING

This appendix is with reference to Sections II and III of the of the main text and explains how the initial conditions for the system (46b) are derived using (46c).

A switch from (46a) to (46b), requires the initial conditions for (46b) ($X_d(\tau_{to})$) to be determined such that the physically observable states/outputs of the system remain continuous. The state vectors X_c and X_d of the dynamics represented in (46a) and (46b) respectively are composed of the following states :

$$X_c = \begin{bmatrix} X & \Delta_c \end{bmatrix}^T = \begin{bmatrix} v_y & \omega_z & y_e & \psi_e & \delta_{c_1} & \delta_{c_2} & \delta_{c_3} & \delta_{c_4} \end{bmatrix}^T \tag{B.1}$$

$$X_d = \begin{bmatrix} X & \Delta_d \end{bmatrix}^T = \begin{bmatrix} v_y & \omega_z & y_e & \psi_e & \delta_{d_1} & \delta_{d_2} & \delta_{d_3} & \delta_{d_4} \end{bmatrix}^T \tag{B.2}$$

where, $X = \begin{bmatrix} v_y & \omega_z & y_e & \psi_e \end{bmatrix}^T$ are the states corresponding to the vehicle dynamics and the tracking error dynamics, and $\Delta_c = \begin{bmatrix} \delta_{c_1} & \delta_{c_2} & \delta_{c_3} & \delta_{c_4} \end{bmatrix}^T$, $\Delta_d = \begin{bmatrix} \delta_{d_1} & \delta_{d_2} & \delta_{d_3} & \delta_{d_4} \end{bmatrix}^T$ are sets of dummy variables for the state space representation of the steering actuator (25) and the driver dynamics (19), as discussed in Section II-B.

The first four states of X_c and X_d are identical, the initial conditions for these states can be formally written as :

$$\begin{bmatrix} 1 & 0 & 0 & 0 & 0 & 0 & 0 & 0 \\ 0 & 1 & 0 & 0 & 0 & 0 & 0 & 0 \\ 0 & 0 & 1 & 0 & 0 & 0 & 0 & 0 \\ 0 & 0 & 0 & 1 & 0 & 0 & 0 & 0 \end{bmatrix} X_d(\tau_{to}) = \begin{bmatrix} 1 & 0 & 0 & 0 & 0 & 0 & 0 & 0 \\ 0 & 1 & 0 & 0 & 0 & 0 & 0 & 0 \\ 0 & 0 & 1 & 0 & 0 & 0 & 0 & 0 \\ 0 & 0 & 0 & 1 & 0 & 0 & 0 & 0 \end{bmatrix} X_c(\tau_{to}) \tag{B.3}$$

The latter set of states, corresponding to $\Delta_c(\tau_{to})$ and $\Delta_d(\tau_{to})$ cannot be equated directly as they do not have a physical meaning and they represent different actuation dynamics. However, the steering angle and its derivatives must remain continuous at the time instant of switching, as it is not physically possible for the driver to apply discontinuous steering inputs. This constraint on the continuity of the steering angle at the time of switching, is imposed up to its third derivative (steering angle, velocity, acceleration and jerk) so as to obtain a set of four equations represented in (27).

Each of the equations in (27) can be written in terms of the state vectors $X_c(\tau_{to})$ and $X_d(\tau_{to})$, starting with the equality between $\delta_c(\tau_{to})$ and $\delta_d(\tau_{to})$, which can be written using (19) and (25) as :

$$\begin{aligned} \delta_c &= \delta_d \\ \implies C_{\Delta_c} X_c &= C_{\Delta_d} X_d \end{aligned} \tag{B.4}$$

N.B. the time argument has been dropped to improve readability.
Taking the time derivative of (B.4) and using the closed loop dymamics (20) and (26), we get :

$$\begin{aligned} \dot{\delta_c} &= \dot{\delta_d} \\ \implies C_{\Delta_c} \dot{X_c} &= C_{\Delta_d} \dot{X_d} \\ \implies C_{\Delta_c}(A_{cc} X_c + B_{cc}\rho) &= C_{\Delta_d}(A_{dc} X_d + B_{dc}\rho) \end{aligned} \tag{B.5}$$

By taking consecutive derivatives of (B.5), the second and third derivatives of δ_c and δ_d can be equated as shown below :

$$\begin{aligned} \ddot{\delta_c} &= \ddot{\delta_d} \\ \implies C_{\Delta_c}(A_{cc}\dot{X_c} + B_{cc}\dot{\rho}) &= C_{\Delta_d}(A_{dc}\dot{X_d} + B_{dc}\dot{\rho}) \\ \implies C_{\Delta_c}(A_{cc}(A_{cc}X_c + B_{cc}\rho) + B_{cc}\dot{\rho}) &= C_{\Delta_d}(A_{dc}(A_{dc}X_d + B_{dc}\rho) + B_{dc}\dot{\rho}) \end{aligned} \tag{B.6}$$

$$\begin{aligned} \dddot{\delta_c} &= \dddot{\delta_d} \\ \implies C_{\Delta_c}(A_{cc}(A_{cc}\dot{X_c} + B_{cc}\dot{\rho}) + B_{cc}\ddot{\rho}) &= C_{\Delta_d}(A_{dc}(A_{dc}\dot{X_d} + B_{dc}\dot{\rho}) + B_{dc}\ddot{\rho}) \\ \implies C_{\Delta_c}(A_{cc}(A_{cc}(A_{cc}X_c + B_{cc}\rho) + B_{cc}\dot{\rho}) + B_{cc}\ddot{\rho}) &= C_{\Delta_d}(A_{dc}(A_{dc}(A_{dc}X_d + B_{dc}\rho) + B_{dc}\dot{\rho}) + B_{dc}\ddot{\rho}) \end{aligned} \tag{B.7}$$

The final expressions of equations (B.4) to (B.7) can be written by collecting the coefficients of X_c, X_d and the input derivatives $\left(\begin{bmatrix}\rho & \dot{\rho} & \ddot{\rho}\end{bmatrix}^T\right)$ as,

$$\begin{aligned}\begin{bmatrix} C_{\Delta_c} \\ C_{\Delta_c}A_{cc} \\ C_{\Delta_c}A_{cc}^2 \\ C_{\Delta_c}A_{cc}^3 \end{bmatrix} X_c + \begin{bmatrix} 0 & 0 & 0 \\ C_{\Delta_c}B_{cc} - C_{\Delta_d}B_{dc} & 0 & 0 \\ C_{\Delta_c}A_{cc}B_{cc} - C_{\Delta_d}A_{dc}B_{dc} & C_{\Delta_c}B_{cc} - C_{\Delta_d}B_{dc} & 0 \\ C_{\Delta_c}A_{cc}^2B_{cc} - C_{\Delta_d}A_{dc}^2B_{dc} & C_{\Delta_c}A_{cc}B_{cc} - C_{\Delta_d}A_{dc}B_{dc} & C_{\Delta_c}B_{cc} - C_{\Delta_d}B_{dc} \end{bmatrix} \begin{bmatrix} \rho \\ \dot{\rho} \\ \ddot{\rho} \end{bmatrix} \\ = \begin{bmatrix} C_{\Delta_d} \\ C_{\Delta_d}A_{dc} \\ C_{\Delta_d}A_{dc}^2 \\ C_{\Delta_d}A_{dc}^3 \end{bmatrix} X_d \end{aligned} \tag{B.8}$$

By combining equations (B.3) and (B.8), the initial conditions for the driver-vehicle system (46b) can be written as :

$$X_d(\tau_{to}) = E^{-1}(FX_c(\tau_{to}) + GP(\tau_{to})) \tag{B.9}$$

where,

$$P = \begin{bmatrix} \rho \\ \dot{\rho} \\ \ddot{\rho} \end{bmatrix}$$

$$E = \begin{bmatrix} 1 & 0 & 0 & 0 & 0 & 0 & 0 & 0 \\ 0 & 1 & 0 & 0 & 0 & 0 & 0 & 0 \\ 0 & 0 & 1 & 0 & 0 & 0 & 0 & 0 \\ 0 & 0 & 0 & 1 & 0 & 0 & 0 & 0 \\ & & & C_{\Delta_d} & & & & \\ & & & C_{\Delta_d}A_{dc} & & & & \\ & & & C_{\Delta_d}A_{dc}^2 & & & & \\ & & & C_{\Delta_d}A_{dc}^3 & & & & \end{bmatrix}, \qquad F = \begin{bmatrix} 1 & 0 & 0 & 0 & 0 & 0 & 0 & 0 \\ 0 & 1 & 0 & 0 & 0 & 0 & 0 & 0 \\ 0 & 0 & 1 & 0 & 0 & 0 & 0 & 0 \\ 0 & 0 & 0 & 1 & 0 & 0 & 0 & 0 \\ & & & C_{\Delta_c} & & & & \\ & & & C_{\Delta_c}A_{cc} & & & & \\ & & & C_{\Delta_c}A_{cc}^2 & & & & \\ & & & C_{\Delta_c}A_{cc}^3 & & & & \end{bmatrix},$$

$$G = \begin{bmatrix} 0 & 0 & 0 \\ 0 & 0 & 0 \\ 0 & 0 & 0 \\ 0 & 0 & 0 \\ 0 & 0 & 0 \\ C_{\Delta_c}B_{cc} - C_{\Delta_d}B_{dc} & 0 & 0 \\ C_{\Delta_c}A_{cc}B_{cc} - C_{\Delta_d}A_{dc}B_{dc} & C_{\Delta_c}B_{cc} - C_{\Delta_d}B_{dc} & 0 \\ C_{\Delta_c}A_{cc}^2B_{cc} - C_{\Delta_d}A_{dc}^2B_{dc} & C_{\Delta_c}A_{cc}B_{cc} - C_{\Delta_d}A_{dc}B_{dc} & C_{\Delta_c}B_{cc} - C_{\Delta_d}B_{dc} \end{bmatrix}$$

as already seen in Section II,

$$\begin{aligned} C_{\Delta_d} &= \begin{bmatrix} 0 & 0 & 0 & 0 & C_d \end{bmatrix} \\ C_{\Delta_c} &= \begin{bmatrix} 0 & 0 & 0 & 0 & C_c \end{bmatrix} \end{aligned} \tag{B.10}$$

where C_d and C_c are the output matrices of the state space realizations of the driver dynamics (19) and the steering actuator dynamics (25) respectively. It is to be noted here that the matrix E in (B.9) has full rank, which can be checked by expanding the last four rows of the matrix E using the expressions for A_{dc} (20) and C_{Δ_d} (B.10), provided (19) is a minimal realization of the transfer function (18).

APPENDIX C
PATH TRACKING CONTROLLER - FEEDBACK GAIN SELECTION

The path tracking controller used in this study is developed in [14] which uses a control law that involves a feedback (δ_{fb}) and a feedforward (δ_{ff}) component. The control law can be written as :

$$\begin{aligned}\delta &= \delta_{fb} + \delta_{ff} \\ &= (k_1 y_e + k_2 \psi_e) + (l + K_\delta u^2)\rho\end{aligned} \tag{C.1}$$

Note that the expression for the feedforward component (δ_{ff}) is discussed in Section II-D.

This Appendix discussed the concept behind determining the feedback gains k_1 and k_2, which is originally proposed in [14].

First, a virtual preview point $\mathcal{P}_a$ is defined at a distance $d_a = l_r + x_{la}$, from the rear axle of the vehicle, as shown in Fig. C.1. Here, x_{la} is the distance of the preview point from the center of mass of the vehicle, which is defined as a function of the forward velocity,

$$x_{la} = h v_x \tag{C.2}$$

in other words, the preview point is h seconds ahead of the vehicle's center of mass.

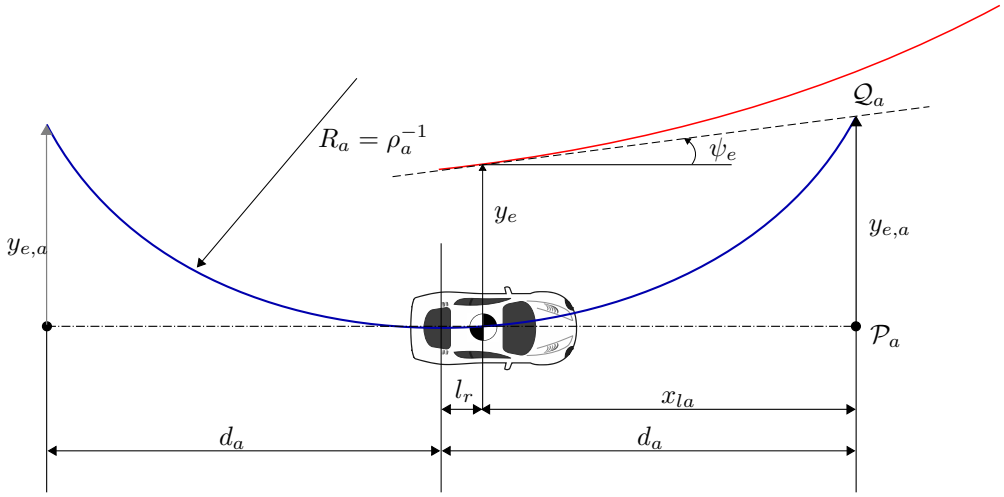

Fig. C.1. Geometric constructions for feedback gain determination. The actual reference path is indicated in red and the newly constructed path is shown in blue.

The orthogonal to the vehicle's longitudinal axis at $\mathcal{P}_a$ meets the tangent to the reference path at a point $\mathcal{Q}_a$, as shown in Fig. C.1. The length of the line segment $\mathcal{P}_a\mathcal{Q}_a$ is defined as an effective lateral error term $y_{e,a}$, given by

$$y_{e,a} := y_e + x_{la} \tan\psi_e \approx y_e + x_{la}\psi_e \tag{C.3}$$

for small values of ψ_e. Now, a new path is constructed for the vehicle to follow, such that it eliminates this effective error $y_{e,a}$. This new path is defined as a circular arc that is tangent to the vehicle's longitudinal axis at the center of its rear axle and passes through the point $\mathcal{Q}_a$, as depicted in Fig. C.1. A circular path is chosen so that the steering angle for steady state cornering (similar to the expression for δ_{ff} in (C.1)) can be used to obtain the steering angle required to follow the newly defined path. Moreover, the center of this circular path is chosen to lie along the rear axle of the vehicle because, the center of rotation of the vehicle also lies approximately along its rear axle for low lateral accelerations.

As $y_{e,a}$ is the Saggita of the new circular path, its radius (R_a) can be derived as,

$$R_a = \frac{y_{e,a}^2 + d_a^2}{2y_{e,a}}$$

for $y_{e,a} \ll d_a$,

$$\rho_a = \frac{1}{R_a} \approx \frac{2y_{e,a}}{d_a^2} \tag{C.4}$$

Note that ρ_a is the curvature of the new circular path that is constructed here and it is different from the curvature of the actual reference path (ρ). This new curvature can now be used to obtain the steady steering angle for following the circular path as,

$$\delta_{fb} = (l + K_\delta v_x^2)\rho_a = \frac{2(l + K_\delta v_x^2)}{d_a^2} y_{e,a} \tag{C.5}$$

Substituting (C.3) in (C.5), the feedback gains k_1 and k_2 in (C.1) can be obtained as :

$$\begin{aligned} k_1 &= \frac{2(l + K_\delta v_x^2)}{d_a^2} \\ k_2 &= \frac{2x_{la}(l + K_\delta v_x^2)}{d_a^2} = \frac{2hv_x(l + K_\delta v_x^2)}{d_a^2} \end{aligned} \tag{C.6}$$

The look ahead time h is a tuning parameter and a larger look value increases the damping of the system as demonstrated in [14]. For a forward speed (v_x) of $100km/h$, the look ahead time is set at 1.5sec. Using the values for the vehicle parameters in Table I in Section II, the feedback gains in (C.6) are obtained as, $k_1 = 0.0081$ and $k_2 = 0.3391$. Furthermore, the feedforward gain k_{ff} in (21) (see Section II-D) is obtained as 0.2742. With this setting the step response of the controller-vehicle closed loop system is shown in Fig. C.2.

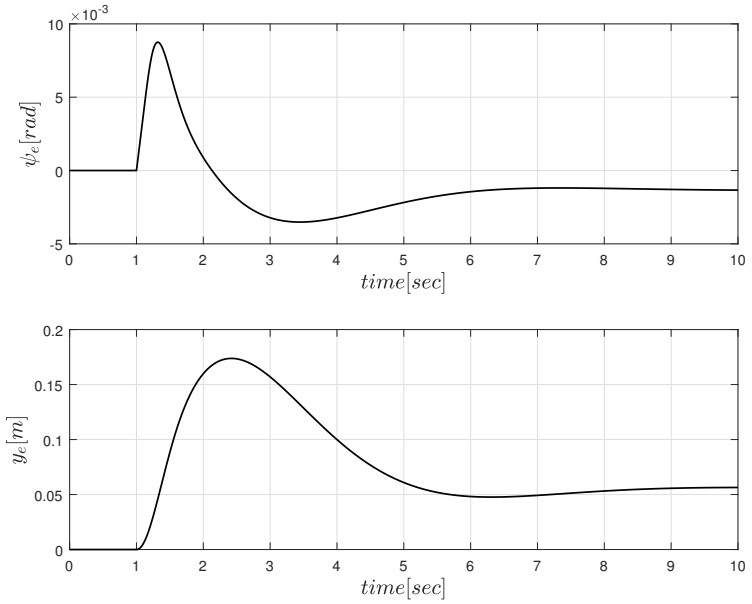

Fig. C.2. Step response of the controller-vehicle closed loop system for a step input of $\rho = \frac{1}{750}m^{-1}$ at $t = 1$sec

It can be seen from Fig. C.2 that the steady state errors are non-zero. It can also be checked from the steady state solution of the vehicle dynamics in (16), that the steady state error in the heading angle (ψ_e^*), is given by,

$$\psi_e^* = \frac{v_y^*}{v_x} = \left(l_r - \frac{l_f m v_x^2}{l C_r}\right)\rho^* \approx \beta^* \tag{C.7}$$

where β^* is the steady state body slip angle and ρ^* is reference curvature at steady state. It can be seen from (C.7) that β^* and hence ψ_e^* has a non zero value for all values of v_x (except for $v_x = \sqrt{l l_r C_r / l_f m}$) which basically indicates that it is not possible for a vehicle to follow a circular path in steady state without a heading error.

Similarly, the steady state lateral tracking error (y_e^*) can also be derived from the vehicle dynamics (16), which also results in a non-zero value at steady state.